

Supporting Information

Crystal engineering of a rectangular sql coordination network to enable xylenes selectivity over ethylbenzene

Naveen Kumar,^{‡a} Shi-Qiang Wang,^{‡a} Soumya Mukherjee,^a Andrey A. Bezrukov,^a Ewa Patyk-Kaźmierczak,^{a,b}
Daniel O’Nolan,^a Amrit Kumar,^a Mei-Hui Yu,^c Ze Chang,^c Xian-He Bu*^c and Michael J. Zaworotko*^a

*E-mail: Michael.Zaworotko@ul.ie

Table of Contents

Hypothetical number of rectangular sql vs. single-linker sql networks (nets)	2
Timeline for sql coordination nets	2
Summary of Crystallographic and topological databases	3
Experimental Section	15
Synthesis of square lattice coordination nets	15
Structural Studies of square lattice coordination nets	16
Single Crystal X-ray Diffraction	16
Characterization and Property Studies of square lattice coordination nets	16
Powder X-ray Diffraction	16
Thermogravimetric Analysis	16
Low Pressure Gas Adsorption Studies	17
Dynamic Vacuum Vapour Sorption	17
C ₈ aromatics selectivity studies	17
Single Crystal X-ray Diffraction data of square lattice coordination nets	19
Powder X-ray Diffraction patterns of square lattice coordination nets	21
Crystallographic analysis of powder X-ray Diffraction data	25
Thermogravimetric Analysis profile	28
Gas Sorption Isotherm	30
Water Vapour Sorption Isotherm	31
Supplement figures of square lattice coordination nets	32
Supplement figures of magnified ¹ H NMR spectrums	34
The summary of adsorbents for adsorptive separation of C ₈ aromatics	40
Summary structural parameters of square lattice coordination nets	41
References	41

Hypothetical number of rectangular sql vs. single-linker sql network (net)s

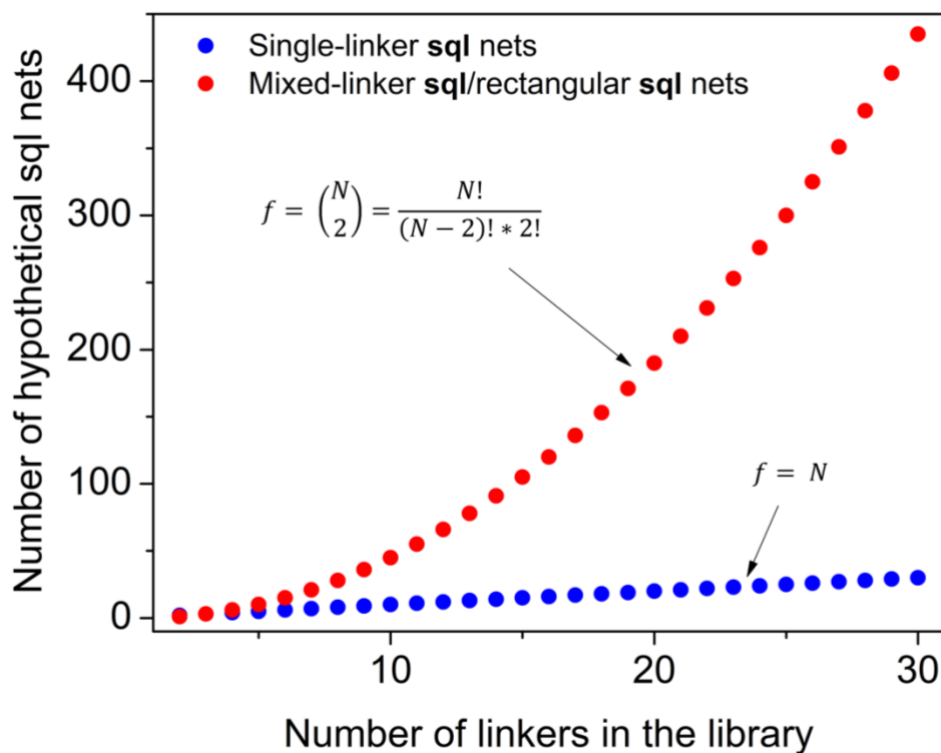


Figure S1. Number of hypothetical mixed-linker sql/rectangular sql and single-linker sql nets as the function of the number of distinct linkers in the library.

Timeline for sql coordination nets

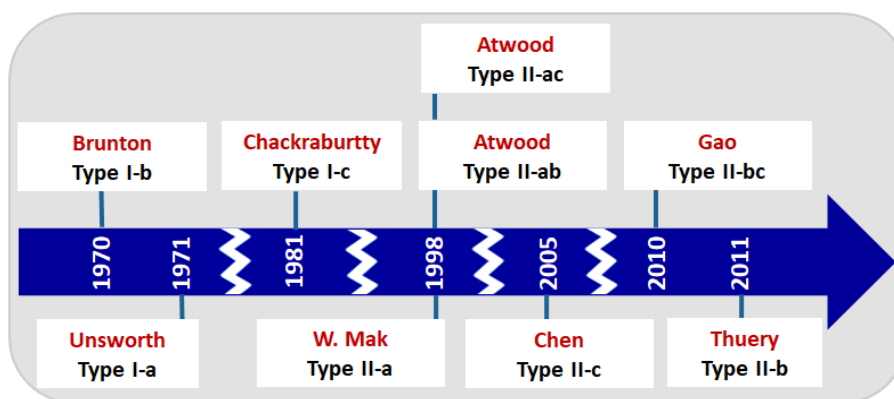


Figure S2. Timeline outlining the emergence of various types of sql coordination nets.

Survey of crystallographic and topological databases

The list of MOMs having **sql** net topology was obtained from the TTO TOPOS database¹ (version: May 2019); valence-bonded MOFs in standard representation were used. The enlisted MOM crystal structures from the TTO database were analyzed using queries to the Cambridge Structural Database (CSD version 5.40, November 2018) through the CSD Application Programming Interface (CSD Python API).²

The analysis was performed using custom-written Python script which implements the algorithm briefly described below. The algorithm comprise of two major steps (Figure S1). In the first step, for 7503 **sql** nets in (CSD database)∩(TTO database) the organic linkers were identified. In the second step, the structures based on commonly occurring organic linkers (linkers listed in Figure 1) were classified as single-linker **sql** nets (type I, Figure 1) or mixed-linker **sql**/rectangular **sql** nets (type II, Figure 1).

First, the organic linkers and their corresponding descriptors were identified for crystal structures by the algorithm. Asymmetric unit of the crystal structure was repeatedly grown (covalent bonds were expanded) on every non-metal atom, ensuring that there is no ‘broken’ ligands and all ligands are accounted in the analysis. In the ‘expanded’ asymmetric unit, the metal atoms and bonds involving metal atoms were removed, thus only organic ligands were left in the structure. Then, for every organic ligand, the non-metal atoms of the ligand coordinating to metal atoms in the parent structure were identified. The organic ligand was considered as a linker, in case the organic ligand was coordinating to at least two different metal atoms through at least two different non-metal atoms. For every linker in the crystal structure, a linker connectivity type (non-metal atom coordinated to the metal, *e.g.* cyclic N, carboxylate O), SMILES representation of the linker structure (if available) and formula of the linker were determined. These descriptors were used in consequent classification steps.

The **sql** net is a mixed-linker net, if there are ≥ 2 distinct organic linkers in the structure. In the classification steps, the set of distinct linkers was determined for **sql** net. The linker was considered as distinct in case it had unique combination of linker descriptors: connectivity, SMILES and formula. Such a strict requirement was applied in order to prevent overlooking the mixed-linker structures, however this strategy resulted in a somewhat high number of false positives due to linker disorder, wrong H modelling, different SMILES representation etc. or a combination thereof. The resulting positives of the automated classification were manually accessed: true positives were classified as mixed-linker **sql** nets, while false positives were classified as single-linker **sql** nets.

Repetitions were treated in the following way. Crystal structures having identical 6-letter part of the CSD RefCode were considered as same structures, thus counted as one structure. This was considered as a viable approach, because such structures had same organic linkers if disorder is ignored (except VASNOT and VASNOT01).

The mixed-linker **sql** nets found by the algorithm are listed in Tables S1-S5 (except type II-ab, where 1300+ nets were found).

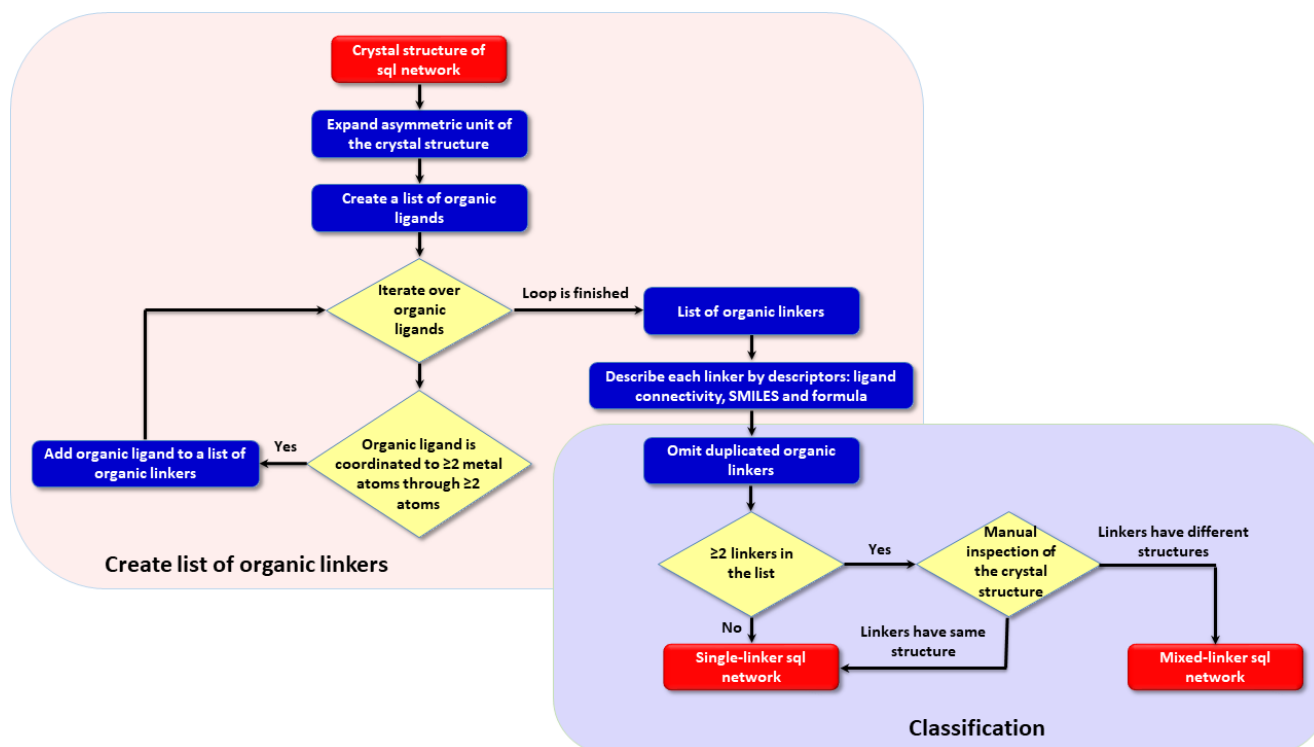


Figure S3. Flow chart of the algorithm used for analysis of sql nets.

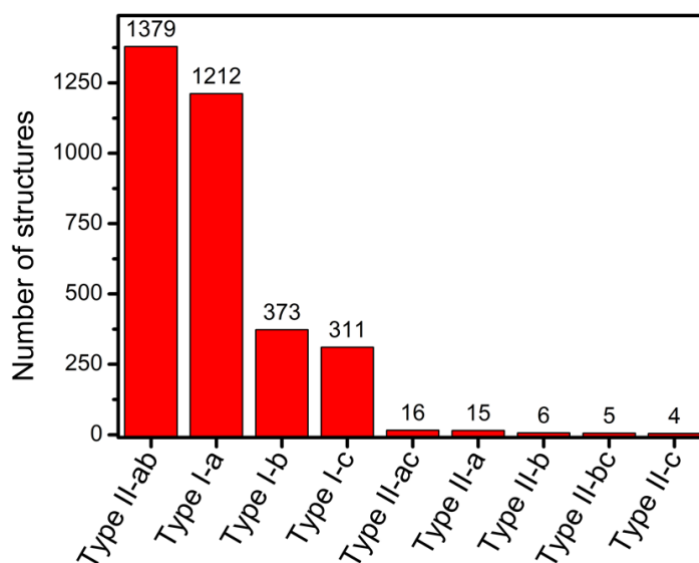
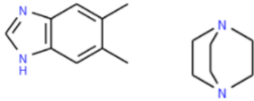
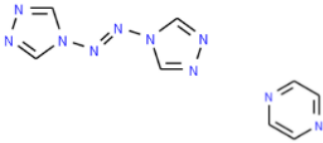
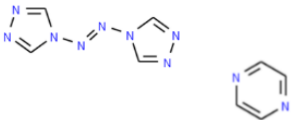
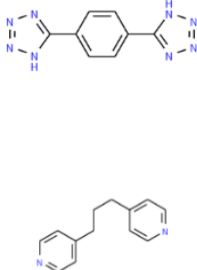
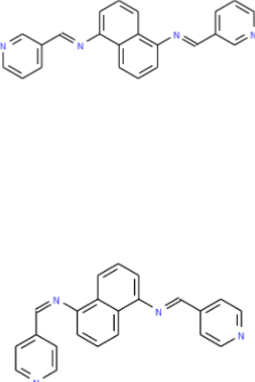
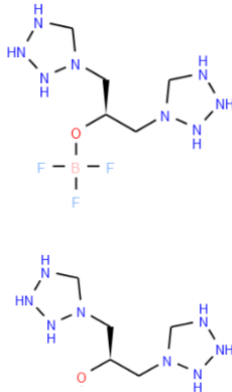
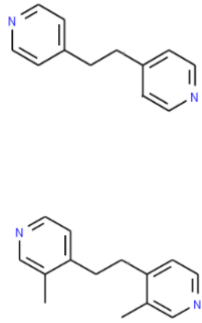
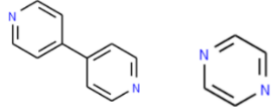
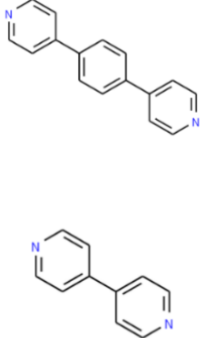
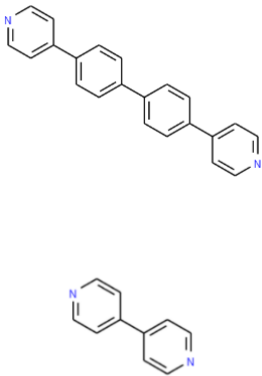
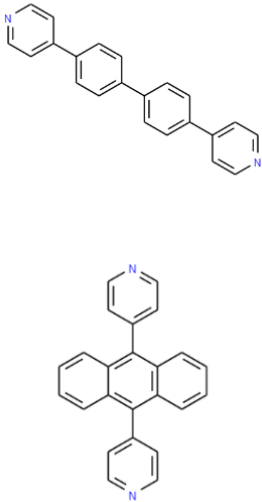
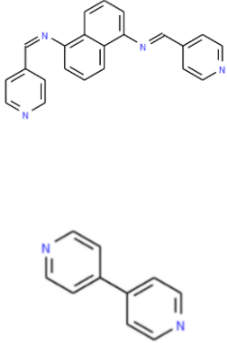
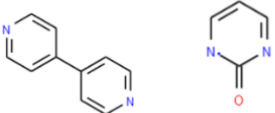


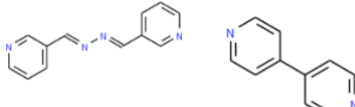
Figure S4. Number of structures reported for different types of sql nets (discussed in the text/manuscript).

Table S1. Type II-a mixed-linker sql/rectangular sql nets found in the database survey.

RefCode	Formula	DOI	Organic linkers
ALIHE J	$(C_{15}H_{21}LiN_4)_n(C_2H_3N)_n$	10.1002/chem.201002316	
BAXG EO	$(C_{10}H_8FeN_{12}S_2)_n[4(H_2O)]_n$	10.1021/ic202626c	
BAXG UE	$(C_{10}H_8FeN_{12}S_2)_n$	10.1021/ic202626c	
BOWQ EK	$(C_{21}H_{18}N_{10}Zn)_n[1.5(H_2O)]_n$	10.1016/j.jssc.2008.12.022	
IZISU G	$(C_{66}H_{48}Cd_2N_{16}O_{12})_n$	10.5012/bkcs.2010.31.9.2668	

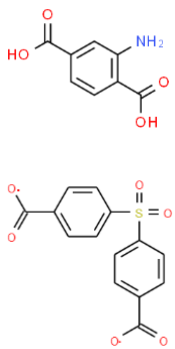
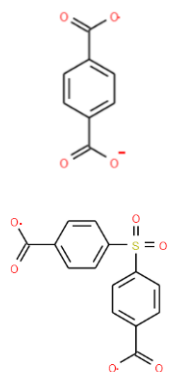
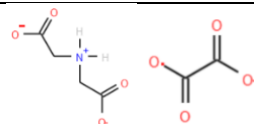
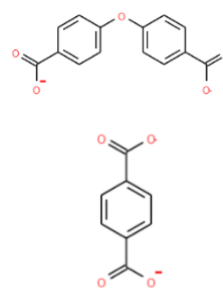
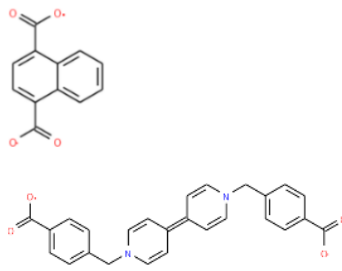
<p>JIMCE O</p>	$(C_{15}H_{23}BF_3FeN_{24}O_{3+})_n(BF_4^-)_n(C_2H_3N)_n[0.8(H_2O)]_n$	<p>10.1016/j.ica.2006. 12.010</p>	
<p>NEHN AQ</p>	$(C_{26}H_{21}CoN_7S_2)_n$	<p>10.1021/cg050439 9</p>	
<p>POWQ EX</p>	$(C_{14}H_{16}CuN_4O_{22+})_n[2(F_6P^-)]_n$	<p>10.1039/a706363f</p>	
<p>QATC UJ</p>	$(C_{26}H_{20}N_6NiO_6)_n[6(C_6H_6)]_n$	<p>10.1039/b007014i</p>	

<p>QATD AQ</p>	$(C_{32}H_{24}N_6NiO_6)_n[8(C_6H_6)]_n$	<p>10.1039/b007014i</p>	
<p>QATD EU*</p>	$(C_{46}H_{34}N_5NiO_{4+})_n(NO_3^-)_n[2(C_6H_6)]_n$	<p>10.1039/b007014i</p>	
<p>TALR EF</p>	$(C_{68}H_{48}Fe_2N_{16}S_4)_n[2.5(CH_2Cl_2)]_n[0.75(H_2O)]_n$	<p>10.1007/s10847-011-0016-5</p>	
<p>TAM WEK</p>	$(C_{68}H_{58}Cl_4Cu_6N_{16}O_{62+})_n[2(NO_3^-)]_n[12.5(H_2O)]_n$	<p>10.1039/b500942a</p>	

TUQSI I	$(C_{22}H_{22}N_6O_2Zn_{2+})_n[(C_{12}H_{10}N_4)]_n(C_{10}H_8N_2)_n[2(ClO_4^-)]_n[2(H_2O)]_n$	10.1016/j.poly.201 0.01.024	
------------	---	--------------------------------	---

* Rectangular **sql** net QATDEU was reported in the same publication as QATCUJ and QATDAQ. The structure was not in the list of **sql** structures obtained from the TOPOS TTO database, therefore it was not found by the script.

Table S2. Type II-b mixed linker sql/rectangular sql nets found in the database survey.

RefCode	Formula	DOI	Organic linkers
CIDCO K	$(C_{22}H_{13}InNO_{10}S^-)_n(C_2H_8N^+)_n$	10.1039/C8DT01405A	
CIDCU Q	$(C_{22}H_{12}InO_{10}S^-)_n(C_2H_8N^+)_n$	10.1039/C8DT01405A	
IXIFEB	$(C_{10}H_{12}N_2O_{12}Th)_n(H_2O)_n$	10.1021/ic102359q	
QAVBO G	$[2(C_2H_8N^+)]_n(C_{22}H_{12}CdO_{92^-})_n$	10.1016/j.inoche.2011.10.039	
YEKNI N	$(C_{38}H_{26}N_2O_8Zn)_n[0.5(C_3H_7NO)]_n[2.5(H_2O)]_n$	10.1002/anie.201203834	

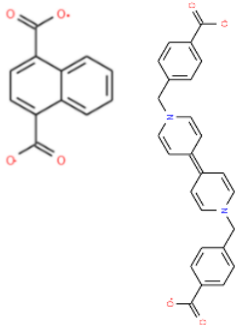
<p>YEKNO T</p>	$(\text{C}_{38}\text{H}_{26}\text{N}_2\text{O}_8\text{Zn})_n[0.5(\text{C}_3\text{H}_6\text{O})]_n[0.5(\text{H}_2\text{O})]_n$	<p>10.1002/anie.201203834</p>	
--------------------	---	-------------------------------	---

Table S3. Type II-c mixed linker sql/rectangular sql nets found in the database survey.

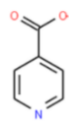
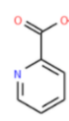
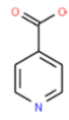
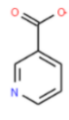
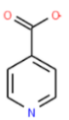
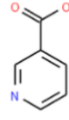
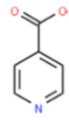
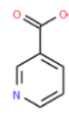
RefCode	Formula	DOI	Organic linkers
DARYEB	$(C_{12}H_{10}CdN_2O_5)_n(H_4N_2)_n$	10.1021/ic0504137	 
NIFKET	$(C_{12}H_8CuN_2O_4)_n$	10.1016/j.inoche.2007.03.019	 
YEVWIG	$(C_{12}H_8N_2O_4Zn)_n$	10.1016/j.molstruc.2006.05.024	 
YEVWOM	$(C_{12}H_8CdN_2O_4)_n$	10.1016/j.molstruc.2006.05.024	 

Table S4. Type II-bc mixed linker sql/rectangular sql nets found in the database survey.

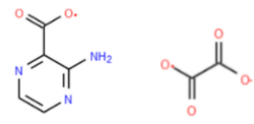
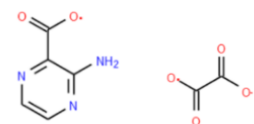
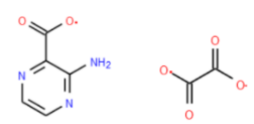
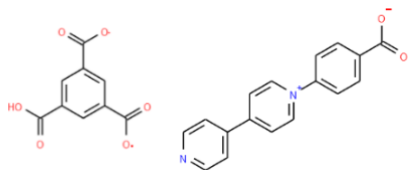
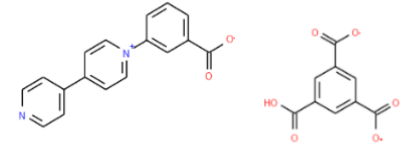
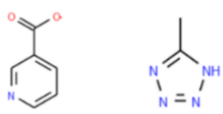
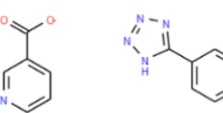
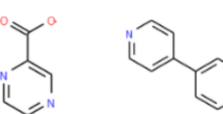
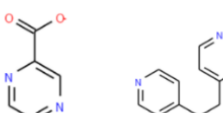
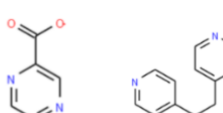
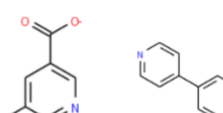
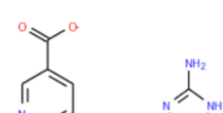
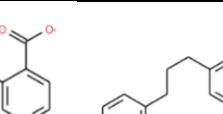
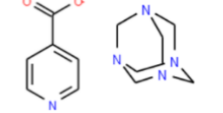
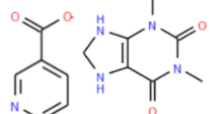
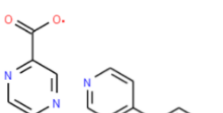
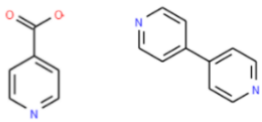
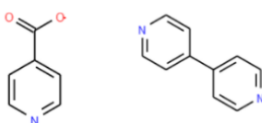
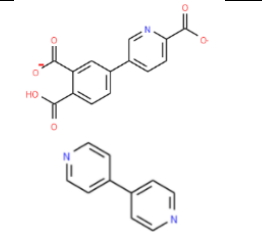
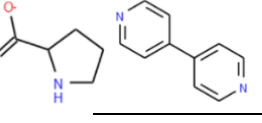
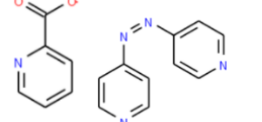
RefCode	Formula	DOI	Organic linkers
AYOGEB	$(C_7H_8LaN_3O_8)_n(H_2O)_n$	10.1107/S1600536811034404	
KAGYOI	$(C_7H_8N_3O_8Pr)_n(H_2O)_n$	10.1039/c0dt00031k	
KAGYUO	$(C_7H_8N_3NdO_8)_n(H_2O)_n$	10.1039/c0dt00031k	
LEKMOG	$(C_{26}H_{16}N_2O_8Zn)_n$	10.1021/acsami.7b13367	
SELQUX	$(C_{26}H_{16}N_2O_8Zn)_n(H_2O)_n$	10.1039/c2cc35115c	

Table S5. Type II-ac mixed linker sql/rectangular sql nets found in the database survey.

RefCode	Formula	DOI	Organic linkers
CILKIT	$(C_8H_7N_5O_2Zn)_n$	10.1016/j.molstruc.2013.09.031	
CUQPUB	$(C_{26}H_{18}N_{10}O_4Zn_2)_n$	10.1021/acs.cgd.5b00637	
FEFTOA	$(C_{15}H_{13}N_4O_3Zn^+)(ClO_4^-)_n(C_2H_6O)_n(H_2O)_n$	10.1002/ejic.200400438	
FEFVAO	$(C_{34}H_{30}N_8O_4Zn_{22+})_n[2(ClO_4^-)]_n[2(C_2H_6O)]_n$	10.1002/ejic.200400438	
FELPES	$(C_{34}H_{30}N_8O_4Zn_{22+})_n[2(ClO_4^-)]_n$	10.1002/ejic.200400438	
FOKKO H	$(C_{34}H_{24}Br_4Cu_2N_6O_{10})_n[5(H_2O)]_n$	10.1016/j.inoche.2014.02.049	
GULBIZ	$(C_7H_6N_6O_2Zn)_n$	10.1016/j.jssc.2009.04.034	
IROSAL	$(C_{20}H_{21}CuN_3O_6)_n[2.5(H_2O)]_n$	10.1021/acs.cgd.6b00610	
QIFNEY	$(C_{12}H_{16}AgN_5O_2)_n[0.5(H_2O)]_n$	10.1039/b009068i	
TEQWIX	$(C_{13}H_{11}N_5O_4Zn)_n$	10.1039/c2nj40625j	
UBUSER	$(C_{16}H_{14}CdN_4O_3)_n[4(H_2O)]_n$	DOI not available, Pei-Xi Lin, Xin-Ping Kang, Zhe An, <i>Wuji Huaxue Xuebao</i> (2011), 27 , 2275	

VALQII	$(C_{16}H_{16}CoN_3O_{4+})_n(C_{10}H_8N_2)_n(NO_3^-)_n[1.5(H_2O)]_n$	10.1021/ja973584m	
VALQO O	$(C_{16}H_{16}CdN_3O_{4+})_n(NO_3^-)_n(C_{10}H_8N_2)_n(H_2O)_n$	10.1021/ja973584m	
VETBII	$(C_{24}H_{17}N_3NiO_7)_n(H_2O)_n$	10.1039/C7CE02009K	
VIHKIH	$(C_{15}H_{16}CdN_4O_5)_n$	10.1039/b706557d	
WIWXE H	$(C_{16}H_{14}MnN_5O_{3+})_n(ClO_4^-)_n(C_2H_6O)_n$	10.1016/j.inoche.2013.12.015	

Experimental Section

All materials were used as received from commercial sources. **4,4'-bipyridyl** (hereafter, abbreviated as **1**) was used as received without any further purification. **(4,4'-bis(4-pyridyl)tetrazine** (hereafter, abbreviated as **3**) was synthesized following a reported procedure.³

Synthesis of square lattice (sql) coordination nets

Solvothermal reaction to scale-up [Co(1)(3)(NCS)₂]_n·2PX, sql-1,3-Co-NCS·2PX

Single crystals of the compound **sql-1,3-Co-NCS·2PX** were obtained by solvothermal reaction as following: a suspension of **3** (0.015 mmol, 3.5 mg), **4,4'-bipyridine** (**1**) (0.015 mmol, 2.3 mg) and Co(NCS)₂ (0.013 mmol, 2.3 mg) in dichloromethane (1 mL), *p*-xylene (1 mL) and MeOH (1 mL) were reacted at 60 °C in a small 10.5 mL glass vial for two days, keeping in a fixed-temperature oven. The crystals were collected in quantitative yield by filtration and washed with *p*-xylene three times.

[Co(1)(3)(NCS)₂]_n·2MX, sql-1,3-Co-NCS·2MX

Single crystals of **sql-1,3-Co-NCS·2MX** were prepared in the same procedure as **sql-1,3-Co-NCS·2PX** via both solvent diffusion and solvothermal, except *m*-xylene was used instead of *p*-xylene.

Single crystals of single-linker sql nets [Co(3)₂(NCS)₂]_n·2OX, sql-3-Co-NCS·2OX and [Co(1)₂(NCS)₂]_n·4OX, sql-1-Co-NCS·4OX

Synthesis of **sql-1,3-Co-NCS·2OX** was attempted using the same synthesis procedure used for **sql-1,3-Co-NCS·2PX** except *o*-xylene was used instead of *p*-xylene. Both solvent diffusion and solvothermal syntheses yielded stoichiometric mixtures of single crystals of **sql-3-Co-NCS·2OX** and **sql-1-Co-NCS·4OX** instead of the desired product **sql-1,3-Co-NCS·2OX**. Unit cell parameters obtained from **sql-1-Co-NCS·4OX** single crystals matched those of our previous report.⁴

Single crystals of single-linker sql nets [Co(3)₂(NCS)₂]_n·2EB, sql-3-Co-NCS·2EB and [Co(1)₂(NCS)₂]_n·2EB, sql-1-Co-NCS·2EB

Synthesis of **sql-1,3-Co-NCS·2EB** was attempted using the same synthesis procedure used for **sql-1,3-Co-NCS·2PX** except ethylbenzene was used instead of *p*-xylene. Both solvent diffusion and solvothermal syntheses yielded stoichiometric mixtures of single crystals of **sql-3-Co-NCS·2EB** and **sql-1-Co-NCS·2EB** instead of the desired product **sql-1,3-Co-NCS·2EB**. Unit cell parameters obtained from **sql-1-Co-NCS·2EB** single crystals matched those of our previous report.⁴

“Single crystals of single-linker sql nets [Co(3)₂(NCS)₂]_n, sql-3-Co-NCS and [Co(1)₂(NCS)₂]_n, sql-1-Co-NCS

Synthesis of **sql-1,3-Co-NCS** was attempted using the same synthesis procedure used for **sql-1,3-Co-NCS·2PX** except no aromatic solvents were used. Both solvent diffusion and solvothermal syntheses yielded a stoichiometric mixture of single crystals of **sql-3-Co-NCS** and **sql-1-Co-NCS** instead of the desired product, **sql-1,3-Co-NCS**. Unit cell parameters obtained from **sql-1-Co-NCS** single crystals matched those of our previous report.⁴”

Structural Studies of square lattice (sql) coordination nets

Single Crystal X-ray Diffraction

Single crystal X-ray diffraction data of all the crystals were collected on a Bruker Quest diffractometer equipped with a μ S microfocus X-ray source (Cu $K\alpha$, $\lambda = 1.54178 \text{ \AA}$) and CMOS detector. APEX3 was used for collecting, indexing, integrating and scaling the data.⁵ Open-flow nitrogen attachment with Oxford Cryosystem was used for low temperature measurements. Absorption correction was performed by multi-scan method.⁶ Space groups were determined using XPREP⁷ as implemented in APEX3. All the scaled data were solved using intrinsic phasing method (XT)⁸ and refined on F_2 using SHELXL⁹ inbuilt in OLEX2 v1.2 (2009) program.¹⁰ All non-hydrogen atoms present in the frameworks were refined anisotropically. Hydrogen atoms were located at idealized positions from the molecular geometry and refined isotropically with thermal parameters based on the equivalent displacement parameters of their carriers. Two of the reported structures were refined from twin crystals. Crystal of **sql-3-Co-NCS·2EB** proved to be an inversion twin (BASF=0.07), whereas that of **sql-3-Co-NCS·2OX** a two domain non-merohedral twin (BASF=0.37), with domains joined with rotation of 180° along direction $[1\bar{1}0]$. Appropriate PART instructions were used to model framework disorder in structures of **sql-1,3-Co-NCS·3EtOH**, **sql-3-Co-NCS·2EB** and **sql-3-Co-NCS·2OX**, and disordered guest molecules in the structures of **sql-3-Co-NCS·2EB** and **sql-3-Co-NCS·2OX**. Due to the low quality of collected data and very complicated disorder of OX molecules in **sql-3-Co-NCS·2OX**; (four OX molecules in the asymmetric part of the unit cell were disordered over nine positions), occupancy of OX molecule at each position was refined individually, rounded up, and then fixed for the final refinement. Where needed, especially for disordered sections of the frameworks and guest molecules, constraints (AFIX) and restraints (SIMU, DELU, ISOR) were used to ensure proper geometry of the molecules, and to allow anisotropic refinement of non-hydrogen atoms. Crystallographic data for all the **sql** coordination nets reported in this paper, are summarized in Tables S6 and S7. All crystal structures have been deposited to the Cambridge Crystallographic Data Centre (CCDC 1916015-1916019, 2006768).

Characterization and Property Studies of square lattice (sql) coordination nets

Powder X-ray Diffraction

Powder X-ray diffraction experiments were conducted using microcrystalline samples on a PANalytical Empyrean diffractometer (40 kV, 40 mA, Cu $K\alpha_{1,2}$, $\lambda = 1.5418 \text{ \AA}$) in Bragg-Brentano geometry. A scan speed of $0.044509^\circ/\text{s}$ ($2.6^\circ/\text{min}$), with a step size of 0.0262° in 2θ was used at room temperature with a range of $5^\circ < 2\theta < 40^\circ$.

Thermogravimetric Analysis (TGA)

TGA for all the compounds, weighing approximately 5-10 mg, were carried out under N₂ atmosphere in a TA Q50 thermal analyzer between room temperature and 550 °C, with a constant heating rate of 10 °C/min.

Low Pressure Gas Adsorption Studies

Low pressure gas adsorption experiments (up to 1 bar) of the activated sample of **sql-1,3-Co-NCS·3EtOH** were conducted on a Micromeritics 3Flex 3500 surface area and pore size analyzer (77 K N₂ and 195 K CO₂). Both samples were degassed under vacuum overnight by using a SmartVacPrep instrument prior to the measurements. Temperature of 77 K for the N₂ sorption experiments were maintained with a 4 L Dewar flask filled with liquid N₂, whereas 195 K CO₂ experiments were recorded with a 4 L Dewar flask filled with a mixture of acetone and dry ice.

Dynamic Vacuum Vapour Sorption

Dynamic vapour sorption measurements were conducted using a Surface Measurement Systems DVS Vacuum at 298 K. Activated samples of **sql-1,3-Co-NCS·3EtOH** were further degassed under high vacuum (1x10⁻⁴ Torr) *in-situ* and stepwise increase in relative pressure were controlled by equilibrated weight changes of the sample (dM/dT = 0.01%/min) from 0 to 95%. Vacuum pressure transducers were used with ability to measure from 1x10⁻⁶ to 760 Torr with a resolution of 0.01%. Approximately 10 mg of sample was used for each experiment. The mass of the sample was determined by comparison to an empty reference pan and recorded by a high resolution microbalance with a precision of 0.1 µg.

C₈ aromatics selectivity studies

Vapour phase: About 30 mg samples of **sql-1,3-Co-NCS** were separately kept in six small vials which stand inside bigger capped/closed vials containing equimolar (5g each) binary of C₈ aromatics (*i.e.* OX/MX, OX/PX, MX/PX, OX/EB, MX/EB and PX/EB) at 85 °C for two days. PXRD patterns (Figure S13) and TGA curves (Figure S21) reveal that **sql-1,3-Co-NCS** completely adsorbed the C₈ aromatics. After that, they were soaked in 5 mL CDCl₃ for two days, enabling the corresponding C₈ aromatics to be completely exchanged by CDCl₃.

Liquid phase: About 30 mg samples of **sql-1,3-Co-NCS** were separately immersed in equimolar (3g each) binary liquid of C₈ aromatics at 85 °C for two days. PXRD patterns (Figures S11 and S12) and TGA curves (Figures S19, S20) reveal that **sql-1,3-Co-NCS** completely adsorbed the C₈ aromatics. Then the saturated samples were filtered and air-dried (*ca.* 10 min) under ambient conditions (*ca.* 20 °C) to remove xylenes adhering to the surface of samples. After that, the samples were soaked in 5 mL CDCl₃ for two days. Apparently color change from dark red to fresh red was observed.

The supernatant of each samples were filtered and collected to measure ¹H NMR spectra (JEOL ECX400 NMR spectrometer). The reliability of NMR has been verified in our recent paper.⁴ The selectivity is defined as:

$$S_{ij} = \frac{x_i y_j}{x_j y_i}$$

where *S* is the selectivity of component *i* relative to component *j*, *x_i* and *x_j* are the mole fractions of components *i* and *j* in the adsorbed phase, and *y_i* and *y_j* are the mole fractions of components *i* and *j* in the liquid phase. For

equimolar binary phase, the selectivity can be simplified as

$$S_{ij} = \frac{x_i}{x_j}$$

The ratio of x_i/x_j can be derived from the integrated area ratio of corresponding methyl groups or methylene group of C₈ aromatics in NMR spectra. When component i and j are both xylene isomers, the selectivity is defined as:

$$S_{ij} = \frac{x_i}{x_j} = \frac{q_i}{q_j}$$

Where q_i and q_j are the relatively integrated area of corresponding methyl groups of xylene isomers. When component i is one of xylene isomers while j is ethylbenzene, the selectivity is defined as:

$$S_{ij} = \frac{x_i}{x_j} = \frac{q_i}{3q_j}$$

Where q_i is the relatively integrated area of corresponding methyl groups (including 6 H) of xylene isomers, while q_j is the relatively integrated area of corresponding methylene group (including 2 H) of ethylbenzene.

Single Crystal X-ray Diffraction data of square lattice coordination nets

Table S6. Crystallographic data of **sql-1,3-Co-NCS·2PX**, **sql-1,3-Co-NCS·2MX** and **sql-1,3-Co-NCS·3EtOH**.

	sql-1,3-Co-NCS·2PX	sql-1,3-Co-NCS·2MX	sql-1,3-Co-NCS·3EtOH
Empirical formula	C ₄₀ H ₃₆ CoN ₁₀ S ₂	C ₄₀ H ₃₆ CoN ₁₀ S ₂	C ₂₄ H ₁₆ CoN ₁₀ S ₂
Formula weight	779.84	779.84	567.52
Temperature/K	301.0	298.32	300.15
Crystal system	Monoclinic	Monoclinic	Monoclinic
Space group	<i>C2/c</i>	<i>C2/c</i>	<i>P2/c</i>
<i>a</i>/Å	24.8225(12)	24.756(2)	10.1578(19)
<i>b</i>/Å	11.4779(5)	11.4713(9)	11.4859(18)
<i>c</i>/Å	14.3010(7)	14.4235(13)	14.985(3)
α/°	90	90	90
β/°	100.423(3)	100.226(4)	106.365(17)
γ/°	90	90	90
Volume/Å³	4007.3(3)	4031.0(6)	1677.5(5)
Z	4	4	4
ρ_{calc}, g/cm³	1.293	1.285	1.124
μ/mm⁻¹	4.660	4.633	5.394
F(000)	518.0	1704.0	578.0
Radiation	CuK α (λ = 1.54178)	CuK α (λ = 1.54178)	CuKα (λ = 1.54178)
Reflections collected	26213	16389	12368
Independent reflections	3090 [R _{int} = 0.0963, R _{sigma} = 0.0505]	1947 [R _{int} = 0.0521, R _{sigma} = 0.0381]	1971 [R_{int} = 0.2551, R_{sigma} = 0.1707]
Data/restraints/parameters	3090/0/244	1947/0/244	1971/78/177
Goodness-of-fit on F²	1.038	1.238	1.071
Final R indexes [I ≥ 2σ(I)]	R ₁ = 0.0562, wR ₂ = 0.1319	R ₁ = 0.0591, wR ₂ = 0.1294	R₁ = 0.1288, wR₂ = 0.3202
Final R indexes [all data]	R₁ = 0.0819, wR₂ = 0.1459	R₁ = 0.0710, wR₂ = 0.1326	R₁ = 0.2123, wR₂ = 0.3534

Table S7. Crystallographic data of single-linker **sql-3-Co-NCS·EB**, **sql-3-Co-NCS·OX** and **sql-3-Co-NCS**.

	sql-3-Co-NCS·2EB	sql-3-Co-NCS·2OX	sql-3-Co-NCS
Empirical formula	C ₄₂ H ₃₆ CoN ₁₄ S ₂	C ₈₄ H ₇₂ Co ₂ N ₂₈ S ₄	C ₂₆ H ₁₆ CoN ₁₄ S ₂
Formula weight	859.90	1719.79	647.58
Temperature/K	150.15	150.01	300.13
Crystal system	Tetragonal	triclinic	orthorhombic
Space group	<i>P4₁22</i>	<i>P-1</i>	<i>Cmca</i>
a/Å	21.7573(4)	13.6994(5)	20.8810(11)
b/Å	21.7573(4)	20.4799(7)	14.7201(9)
c/Å	20.5483(5)	21.1055(7)	8.7578(5)
α/°	90	78.892(2)	90
β/°	90	73.265(2)	90
γ/°	90	79.327(2)	90
Volume/Å³	9727.2(4)	5511.1(3)	2691.9(3)
Z	8	2	4
ρ_{calc.} g/cm³	1.174	1.036	1.598
μ/mm⁻¹	3.912	3.452	6.852
F(000)	3560.0	1780.0	1316.0
Radiation	CuKα (λ = 1.54178)	CuKα (λ = 1.54178)	CuKα (λ = 1.54178)
Reflections collected	166061	13415	5637
Independent reflections	7433 [R _{int} = 0.1745, R _{sigma} = 0.0644]	13415 [R _{int} = 0.1743, R _{sigma} = 0.1287]	1045 [R_{int} = 0.0835, R_{sigma} = 0.0536]
Data/restraints/parameters	7433/601/707	13415/1101/1440	1045/0/104
Goodness-of-fit on F₂	1.066	1.039	1.069
Final R indexes [I >= 2σ (I)]	R ₁ = 0.1192, wR ₂ = 0.2673	R ₁ = 0.1356, wR ₂ = 0.3066	R₁ = 0.0519, wR₂ = 0.1278
Final R indexes [all data]	R₁ = 0.1583, wR₂ = 0.2908	R₁ = 0.2223, wR₂ = 0.3684	R₁ = 0.0788, wR₂ = 0.1458

Powder X-ray Diffraction

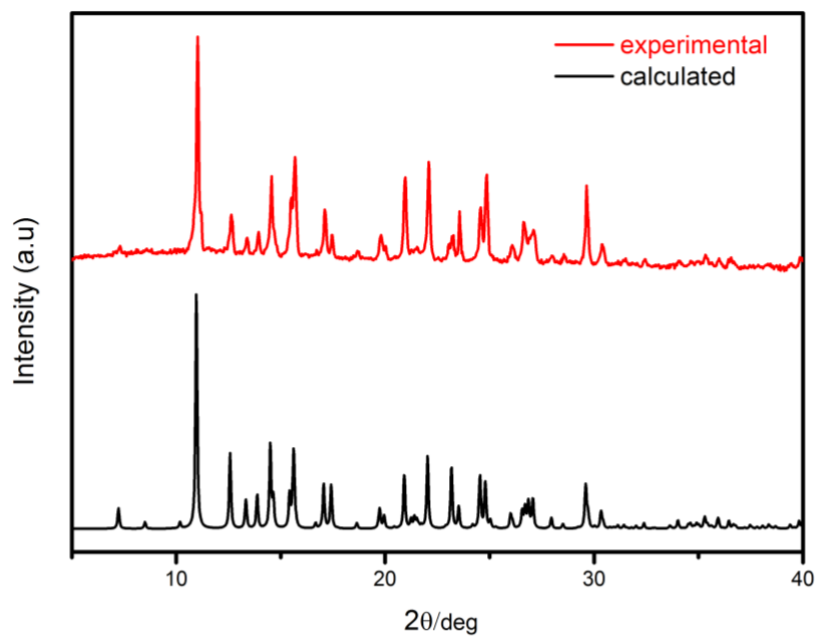


Figure S5. PXRD patterns of **sql-1,3-Co-NCS·2PX**.

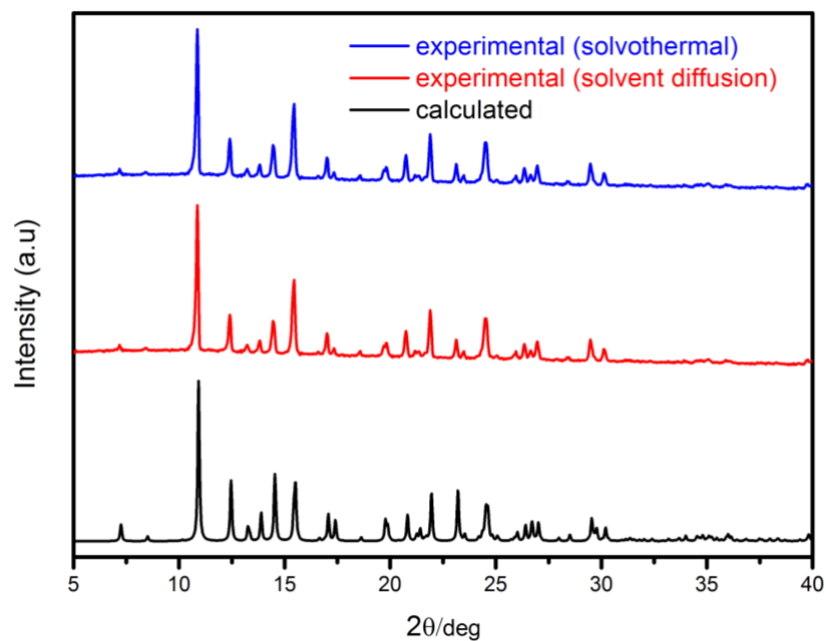


Figure S6. PXRD patterns of **sql-1,3-Co-NCS·2MX**.

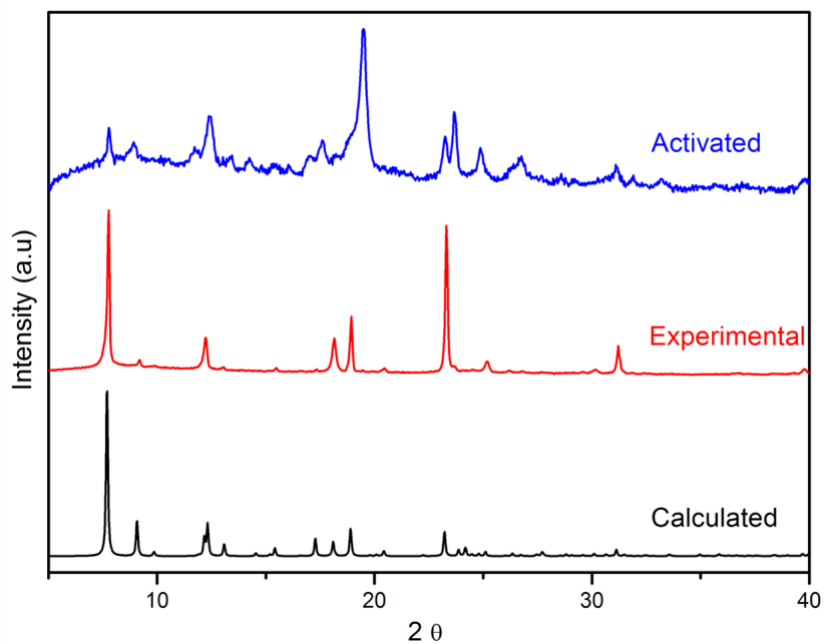


Figure S7. PXRD patterns of **sql-1,3-Co-NCS·3EtOH** and its corresponding activated phase.

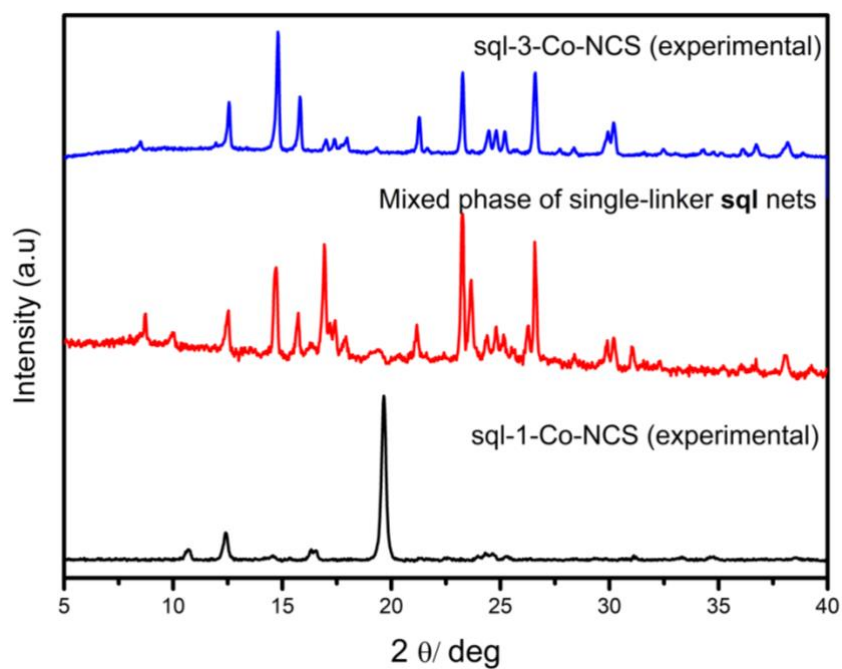


Figure S8. PXRD patterns collected during trial experiments to synthesize **sql-1,3-Co-NCS**, without using any aromatic solvent/template and that of the obtained mixed phase of single-linker **sql** nets.

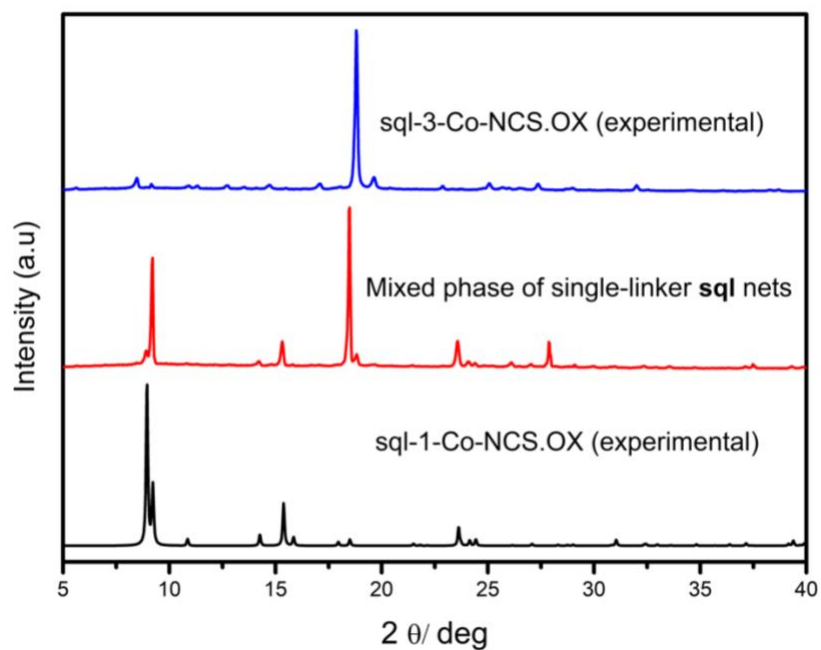


Figure S9. PXRD patterns from trial experiments to synthesize **sql-1,3-Co-NCS·2OX**, and that of the obtained mixed phase of single-linker **sql** nets.

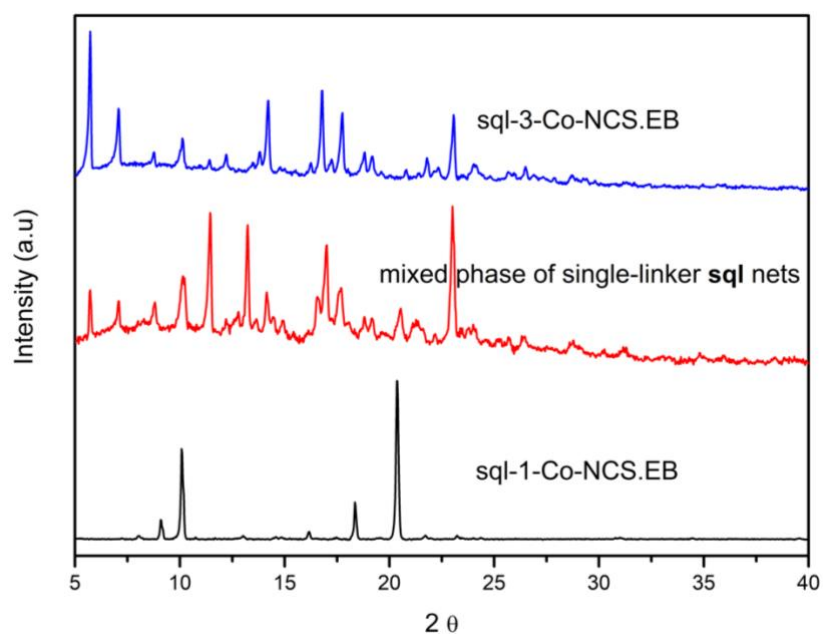


Figure S10. PXRD patterns from trial experiments to synthesize **sql-1,3-Co-NCS·EB**, and that of the obtained mixed phase of single-linker **sql** nets.

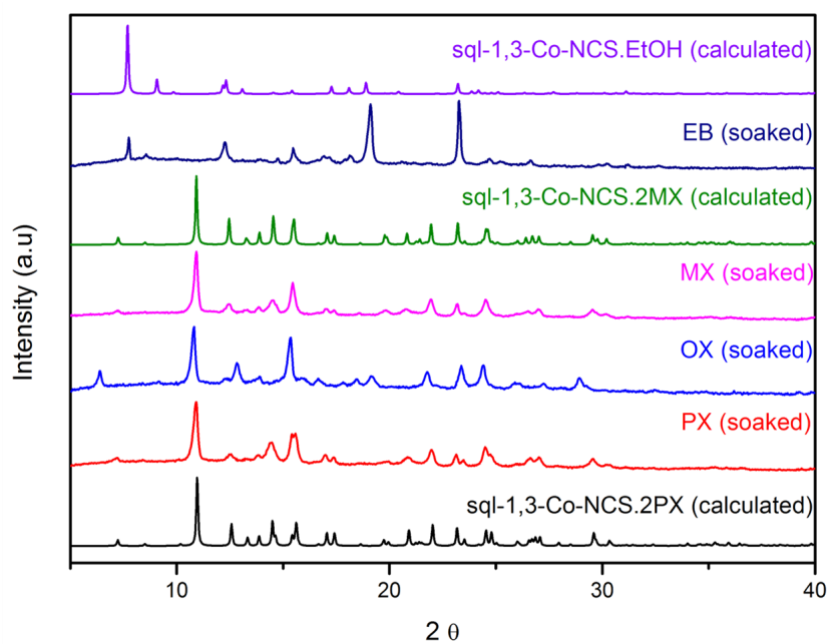


Figure S11. PXRD patterns for the solvent soaking experiments in pure xylenes and ethylbenzene.

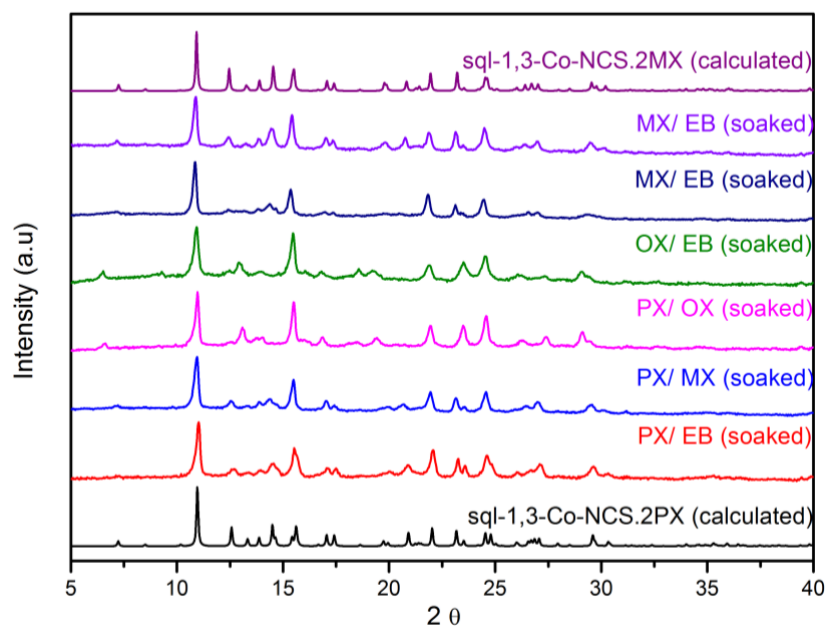


Figure S12. PXRD patterns obtained on soaking of the activated samples in binary mixtures of xylenes and ethylbenzene.

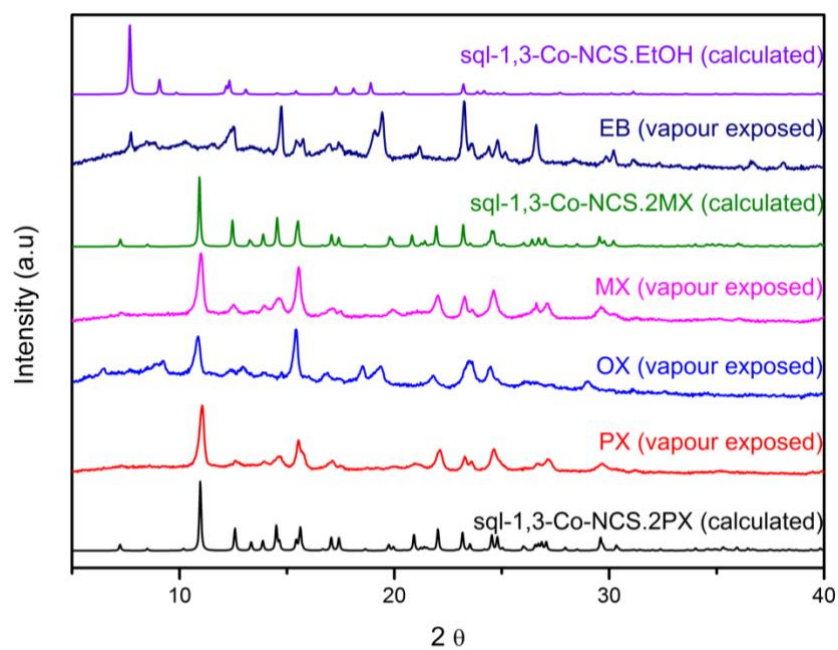


Figure S13. PXRD patterns obtained after exposing pure xylenes and EB vapour to the activated samples.

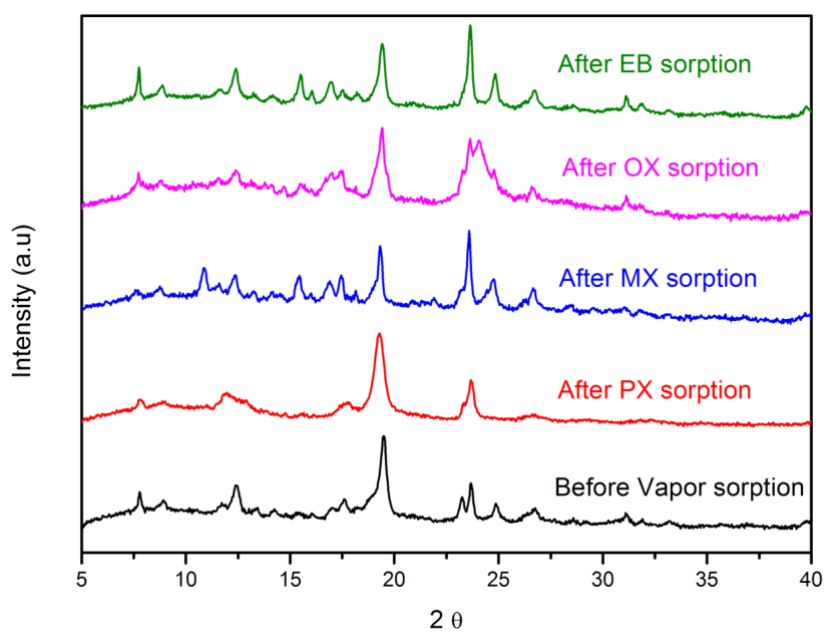


Figure S14. PXRD patterns of the activated samples of **sql-1,3-Co-NCS·3EtOH**, before and after vapour sorption.

Crystallographic analysis of powder X-ray Diffraction data

Table S8. Unit cell parameters determined from powder X-ray diffraction data

Phase	sql-1,3-Co-NCS·nCO ₂	sql-1,3-Co-NCS·2OX
Temperature/K	195	298
Crystal system	Monoclinic	Monoclinic
Space group	<i>P2/c</i>	<i>P2</i>
<i>a</i> /Å	10.439(3)	25.00(8)
<i>b</i> /Å	11.5752(9)	11.53(11)
<i>c</i> /Å	14.824(4)	14.05(3)
α /°	90	90
β /°	105.897(9)	100.3(3)
γ /°	90	90
Volume/Å ³	1722.74(18)	3986(6)
<i>wR</i> ₂	1.04 %	2.37 %
<i>RF</i> ₂	5.30%	34.5 %

Determination of unit cell parameters of sql-1,3-Co-NCS·nCO₂.

The unit cell parameters of **sql-1,3-Co-NCS·nCO₂** were determined from the powder X-ray diffraction pattern collected at 195 K in CO₂ atmosphere (*P* = 90 kPa). Positions of the first 14 peaks were used as the input data for indexing purpose, using DICVOL¹¹ implemented in DASH.¹² Pawley profile fit of the whole powder X-ray diffraction pattern was performed using GSASII¹³ (Figure S15). The refined unit cell parameters are: *a* = 10.439(3) Å, *b* = 11.5752(9) Å, *c* = 14.824(4) Å, β = 105.897(9) °, *V* = 1722.74(18) Å³, *wR* = 1.04 %, *RF*₂ = 5.30%.

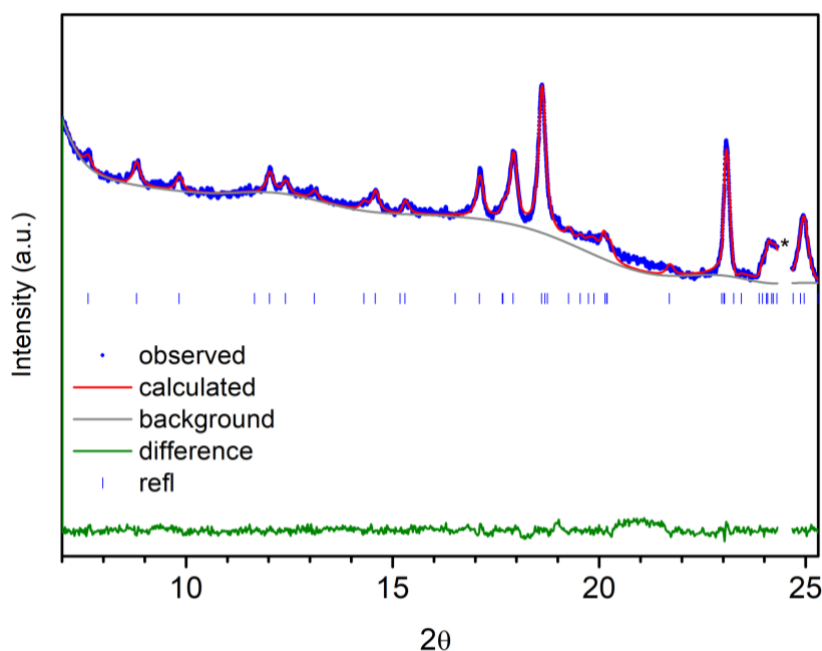


Figure S15. Pawley profile fit for the PXRD pattern of **sql-1,3-Co-NCS·nCO₂**. *Corresponding region (from 24.3 to 24.7 ° 2θ) is excluded from the refinement because of the peak belonging to dry ice (e.g. COD (Crystallography Open Database) entry #1010489).

Determination of unit cell parameters of **sql-1,3-Co-NCS·2OX**

Unit cell parameters of **sql-1,3-Co-NCS·2PX** were used as initial guess for Pawley profile fit of the PXRD pattern of **sql-1,3-Co-NCS·2OX** (Figure S16).

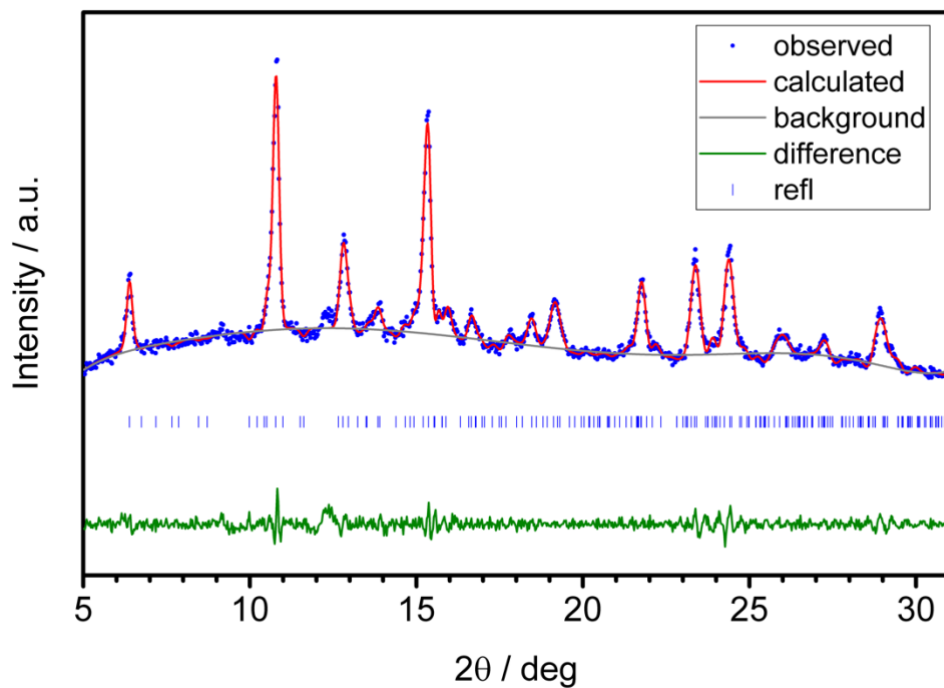


Figure S16. Pawley profile fit of the PXRD pattern of **sql-1,3-Co-NCS·2OX**.

Thermogravimetric Analysis profile

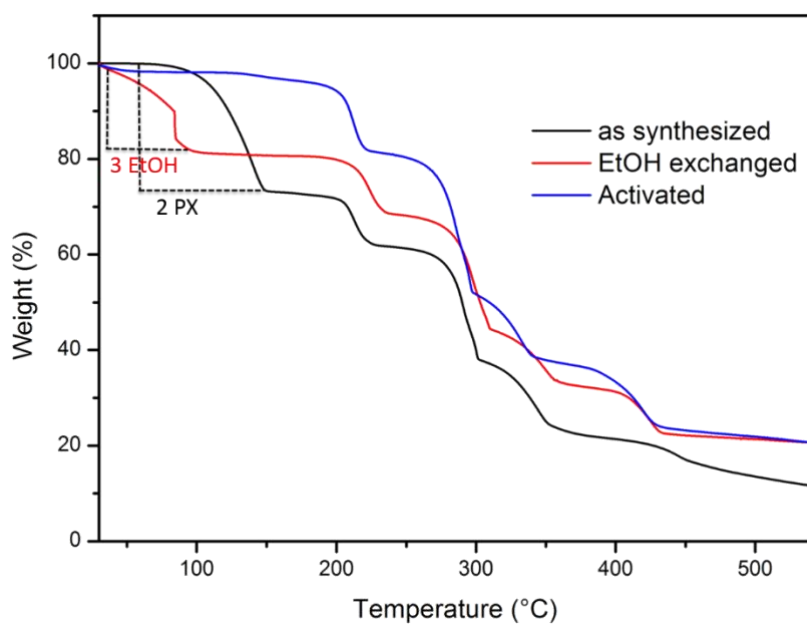


Figure S17. TGA profiles for the as-synthesized, EtOH exchanged and activated samples of $\text{sql-1,3-Co-NCS}\cdot 2\text{PX}$.

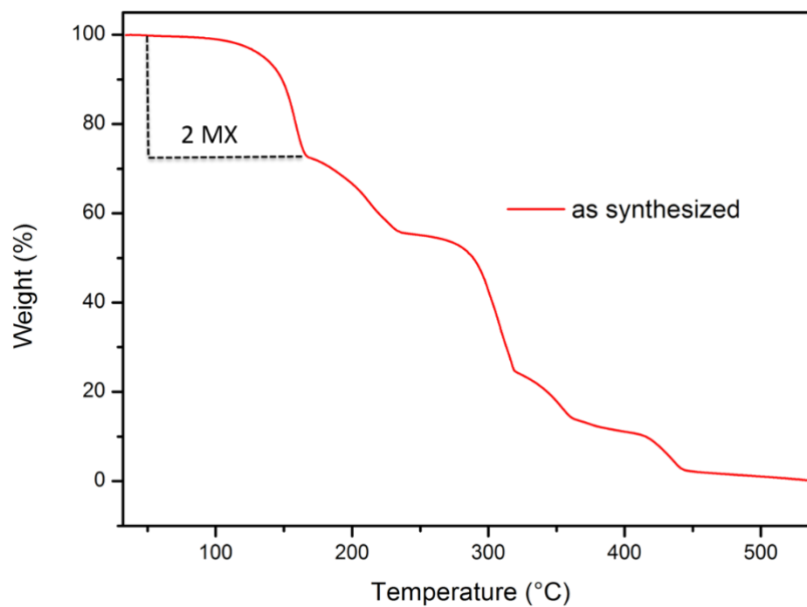


Figure S18. TGA profiles for the as synthesized $\text{sql-1,3-Co-NCS}\cdot 2\text{MX}$.

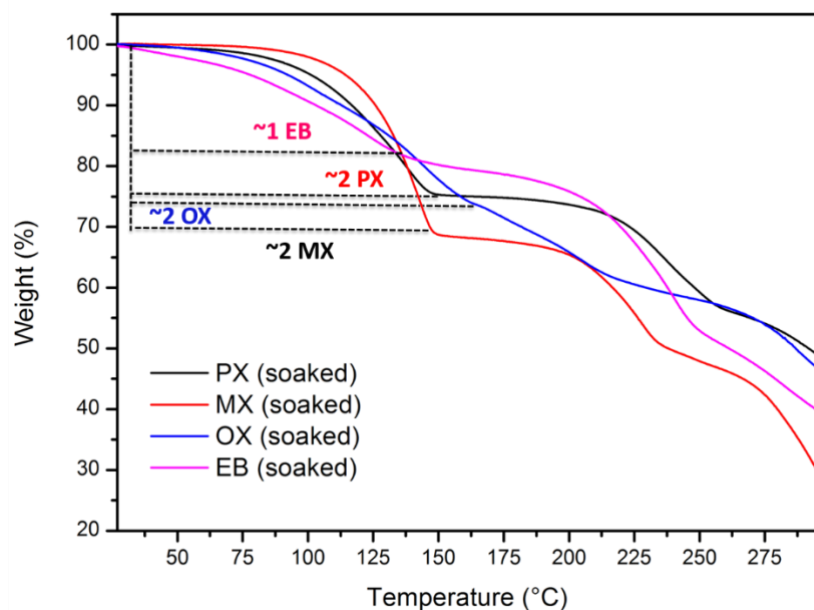


Figure S19. TGA profiles for the solvent soaking experiments, after soaking in xylenes and ethylbenzene.

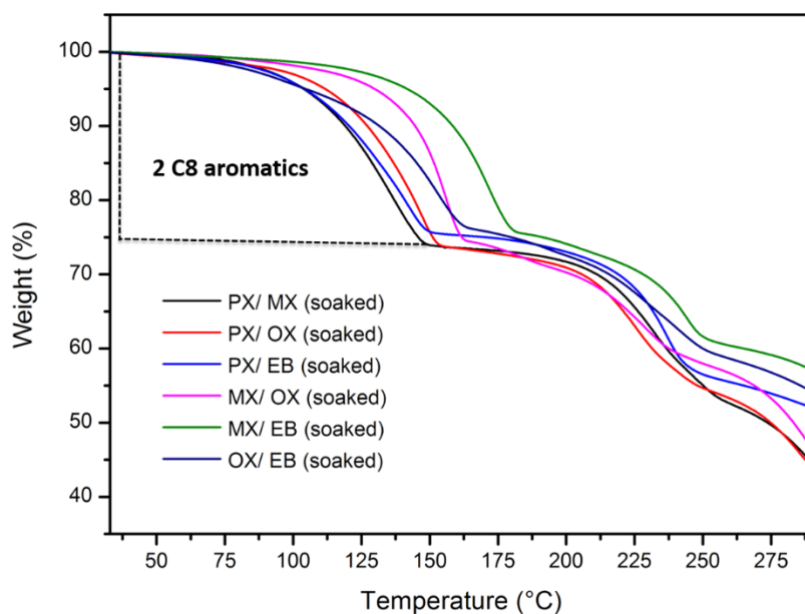


Figure S20. TGA profiles for the solvent soaking experiments, after soaking the activated samples in binary (1:1) mixtures of xylenes and ethylbenzene.

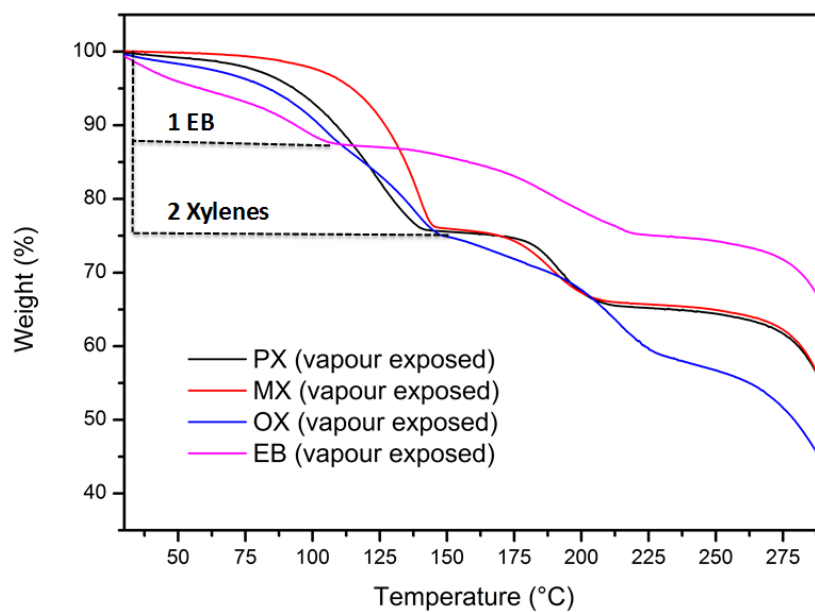


Figure S21. TGA profiles for the vapour exposed experiments, after exposing to pure xylenes and EB vapour.

Gas Sorption Isotherms

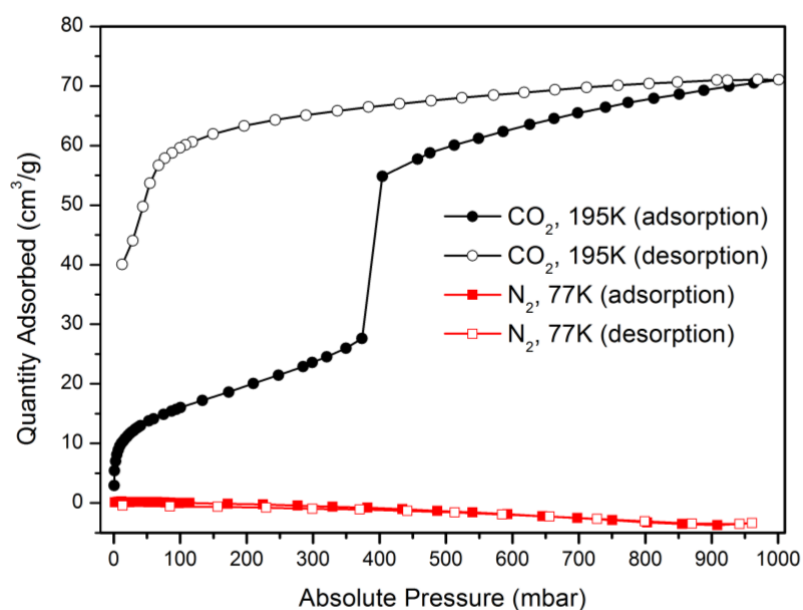


Figure S22. CO₂ and N₂ isotherms recorded at 195 K and 77 K respectively, for **sql-1,3-Co-NCS·3EtOH**.

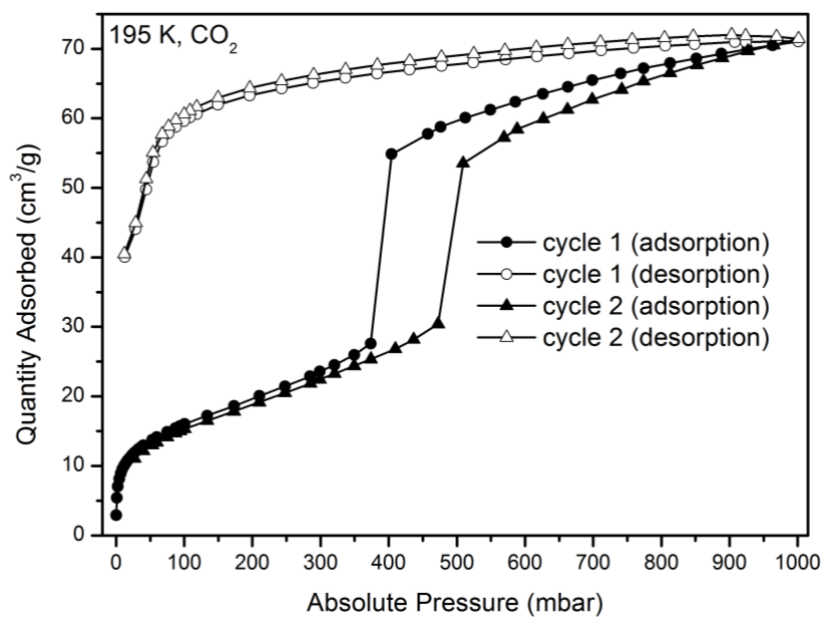


Figure S23. CO₂ isotherms at 195 K for the activated **sql-1,3-Co-NCS·3EtOH**, recorded over two consecutive cycles.

Water vapour sorption Isotherm

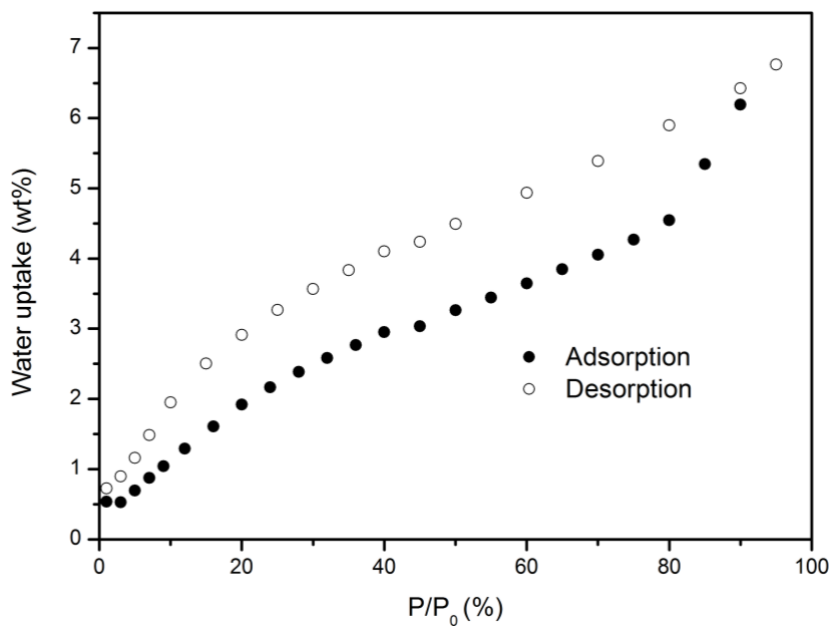


Figure S24. Water vapour sorption isotherm at 300 K for the activated sample of **sql-1,3-Co-NCS·3EtOH**.

Supplementary figures of the square lattice coordination nets

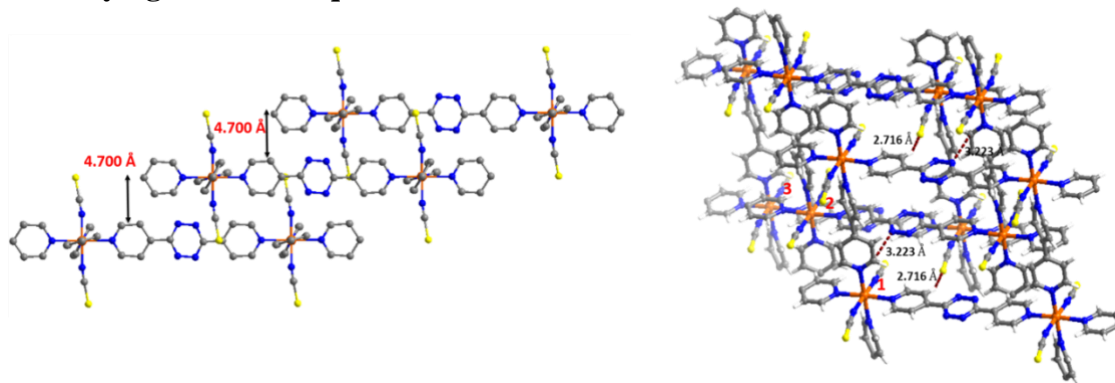


Figure S25. Crystal structure of **sql-1,3-Co-NCS·3EtOH** depicting: left: layer packing arrangement; right: host-host interactions exhibiting C-H...S hydrogen bonds between layers 1 and 3; also, C-H... π interactions between nets 1 & 2 and 2 & 3.

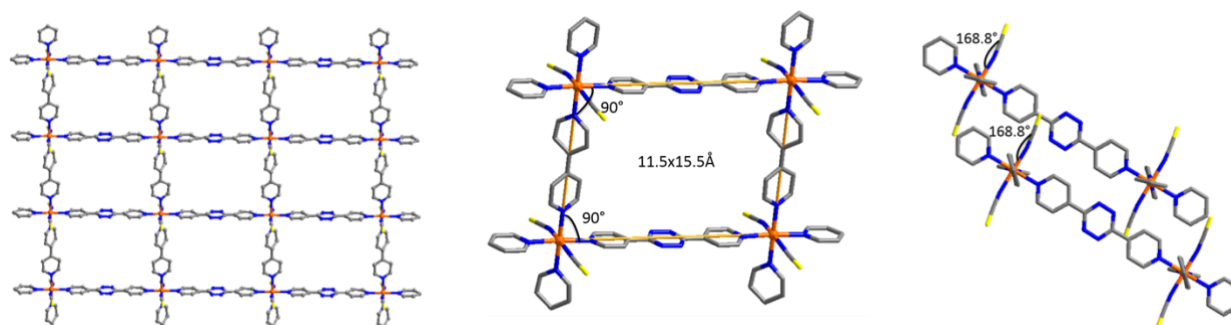


Figure S26. Crystal structure of **sql-1,3-Co-NCS·3EtOH** depicting the square grids and layer packing.

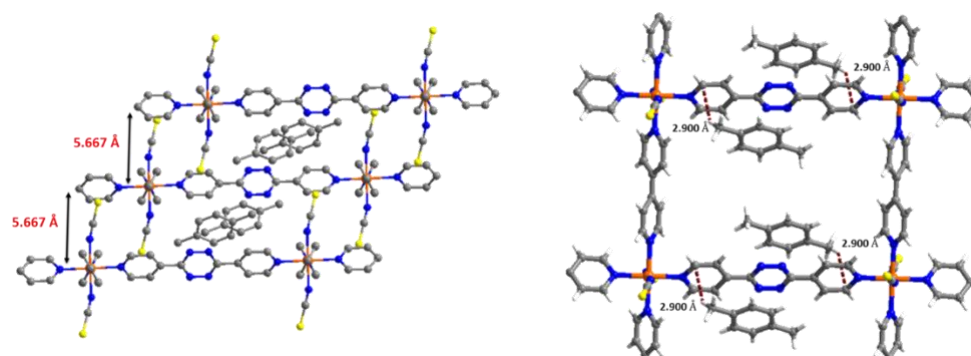


Figure S27. Crystal structure of **sql-1,3-Co-NCS·2 p-xylene** depicting: left: layer packing arrangement; right: host-guest interactions showing C-H... π interactions.

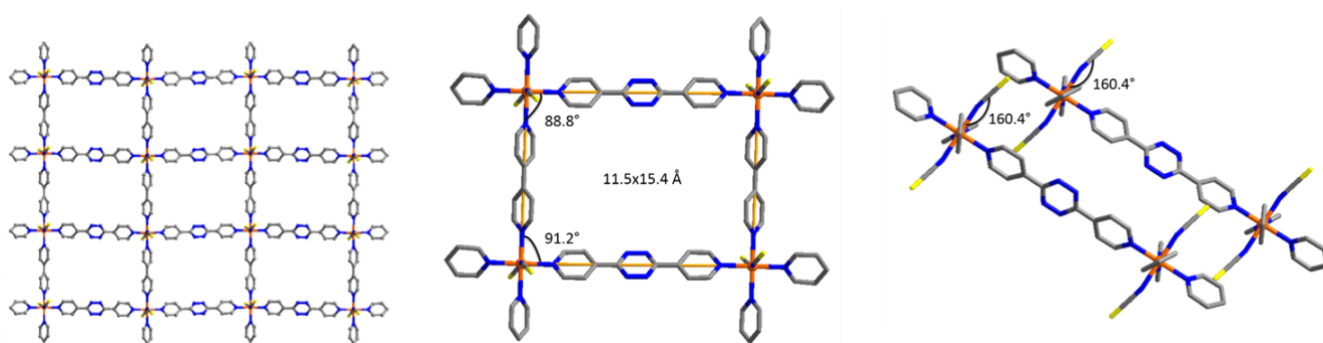


Figure S28. Crystal structure of **sql-1,3-Co-NCS·2 *p*-xylene** depicting the square grids and layer packing.

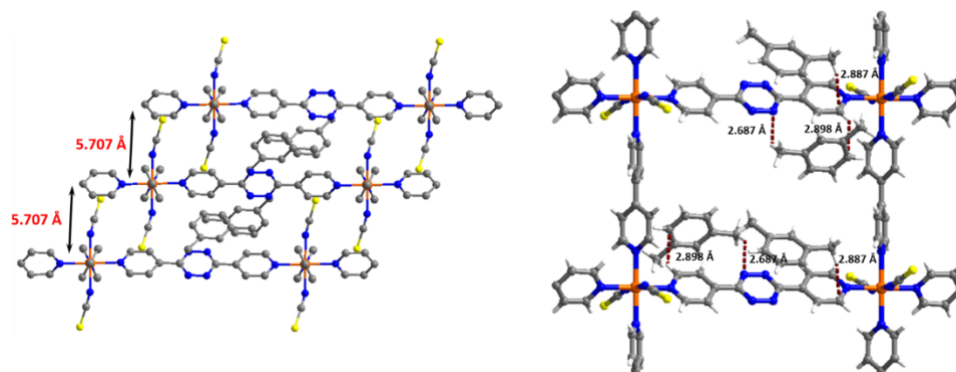


Figure S29. Crystal structure of **sql-1,3-Co-NCS·2 *m*-xylene** depicting: left: layer packing arrangement; right: host-guest interactions showing C-H... π interactions.

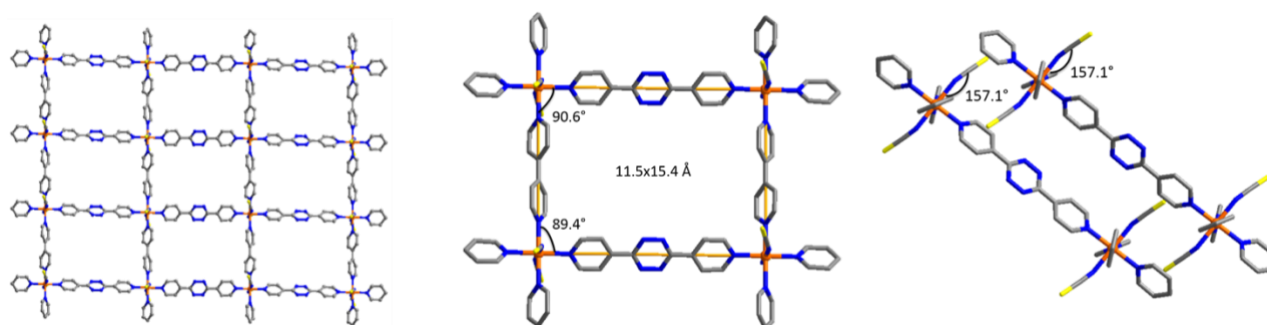


Figure S30. Crystal structure of **sql-1,3-Co-NCS·2 *m*-xylene** depicting the square grids and layer packing.

Supplementary figures for magnified ^1H NMR spectrums

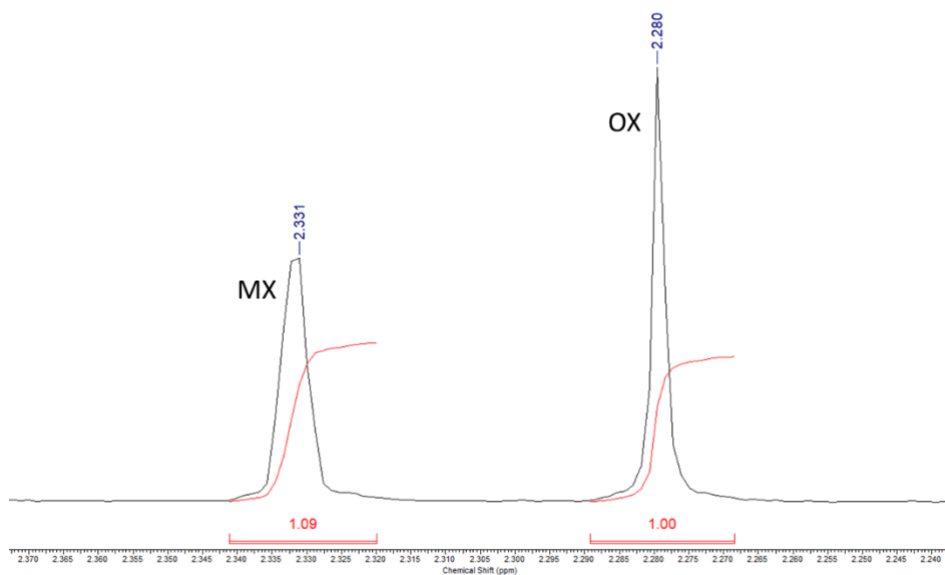


Figure S31. Magnified ^1H NMR spectrum recorded using the CDCl_3 extract of C_8 aromatics obtained from **sql-1,3-Co-NCS** that was prior subjected to the equimolar binary vapour of OX/MX until saturated.

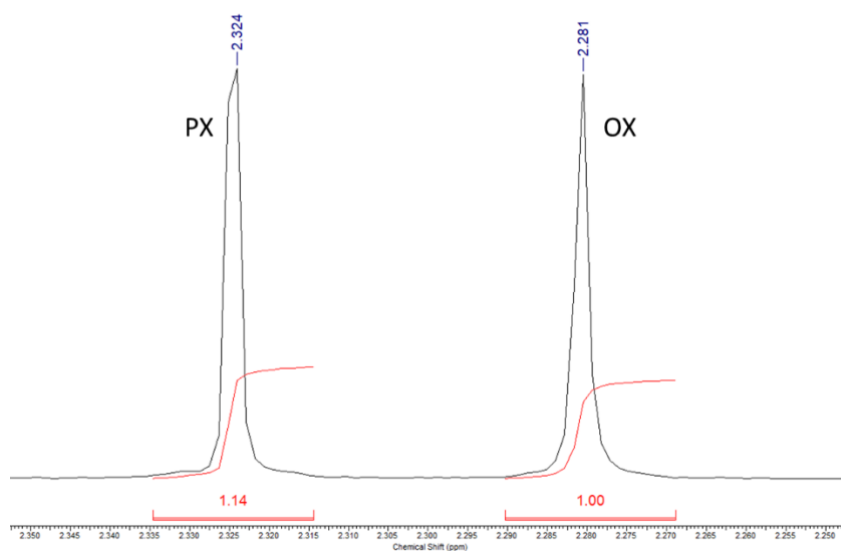


Figure S32. Magnified ^1H NMR spectrum recorded using the CDCl_3 extract of C_8 aromatics obtained from **sql-1,3-Co-NCS** that was prior subjected to the equimolar binary vapour of OX/PX until saturated.

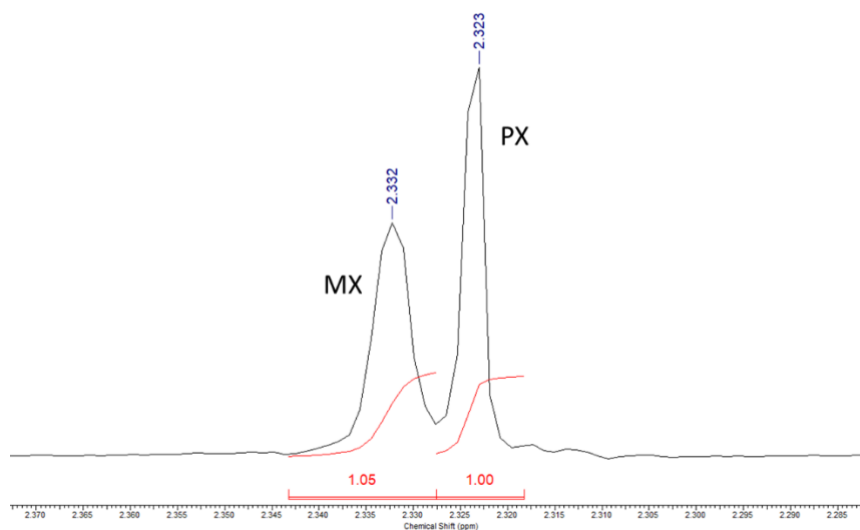


Figure S33. Magnified ¹H NMR spectrum recorded using the CDCl₃ extract of C₈ aromatics obtained from sql-1,3-Co-NCS that was prior subjected to the equimolar binary vapour of PX/MX until saturated.

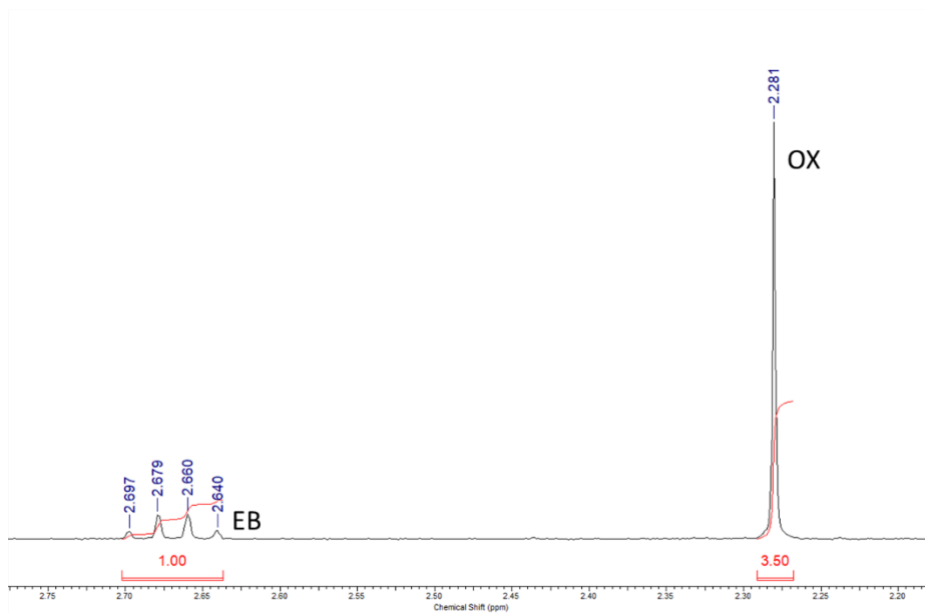


Figure S34. Magnified ¹H NMR spectrum recorded using the CDCl₃ extract C₈ aromatics from sql 1,3-Co-NCS that was prior subjected to the equimolar binary vapour of OX/EB until saturated.

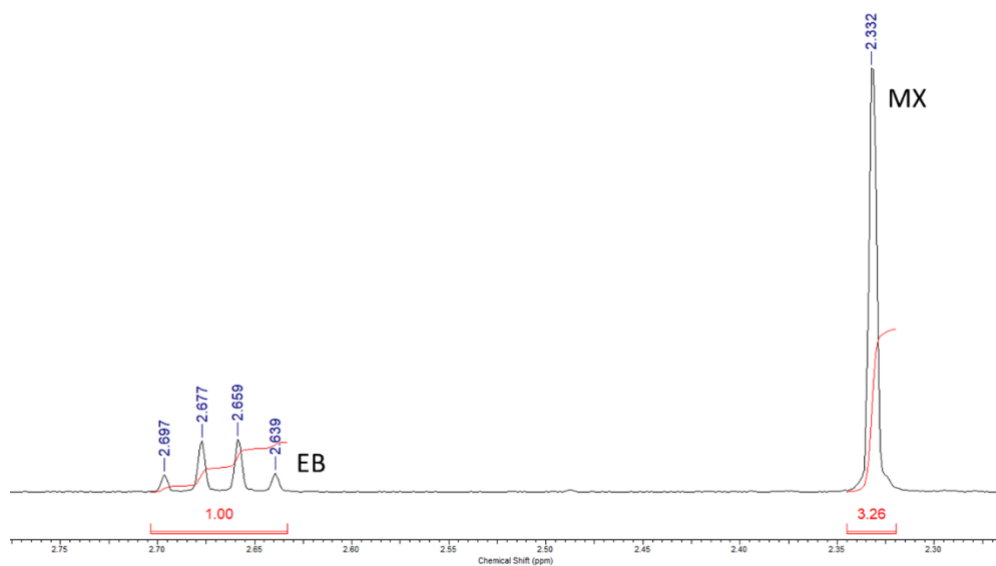


Figure S35. Magnified ^1H NMR spectrum recorded using the CDCl_3 extract C_8 aromatics from **sql-1,3-Co-NCS** that was prior subjected to the equimolar binary vapour of MX/EB until saturated.

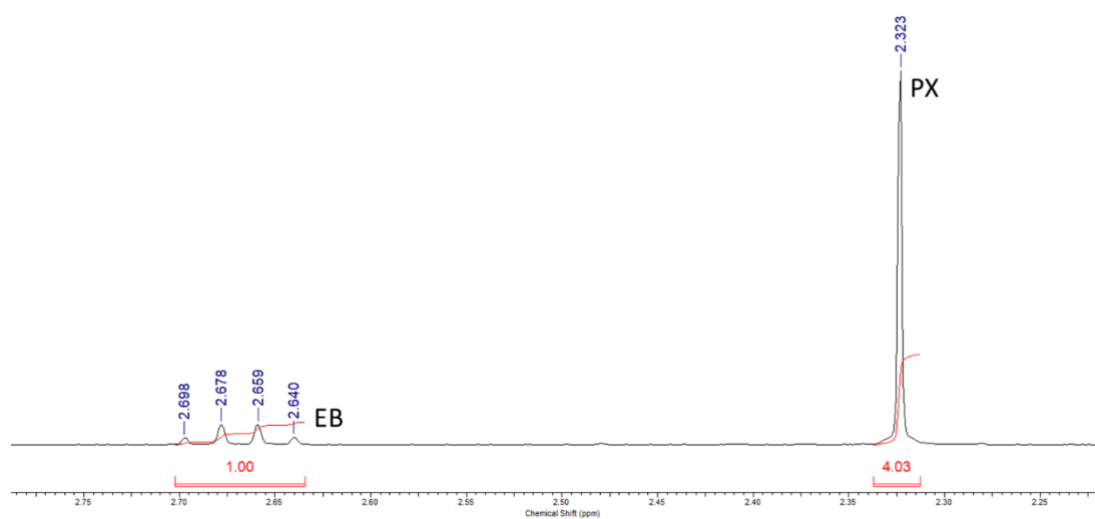


Figure S36. Magnified ^1H NMR spectrum recorded using the CDCl_3 extract C_8 aromatics from **sql-1,3-Co-NCS** that was prior subjected to the equimolar binary vapour of PX/EB until saturated.

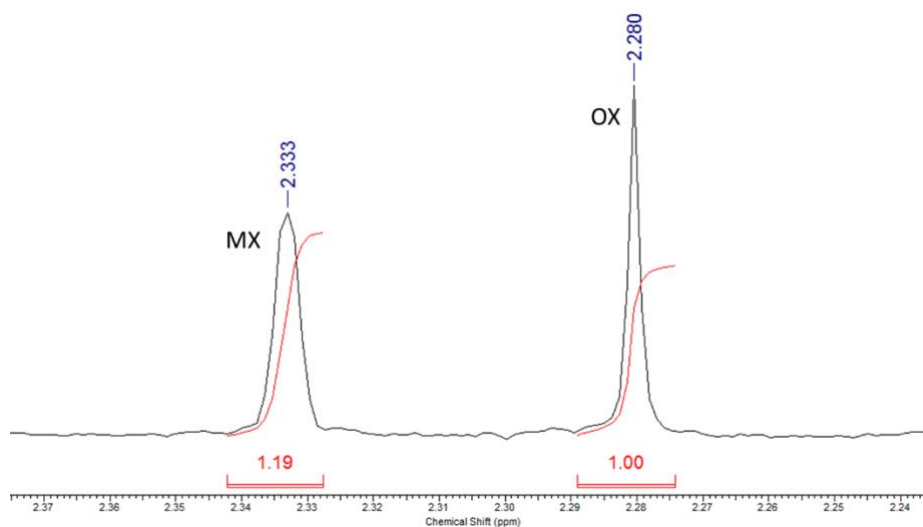


Figure S37. Magnified ¹H NMR spectrum recorded using the CDCl₃ extract of C₈ aromatics obtained from **sql-1,3-Co-NCS** that was prior subjected to the equimolar binary liquid of OX/MX until saturated.

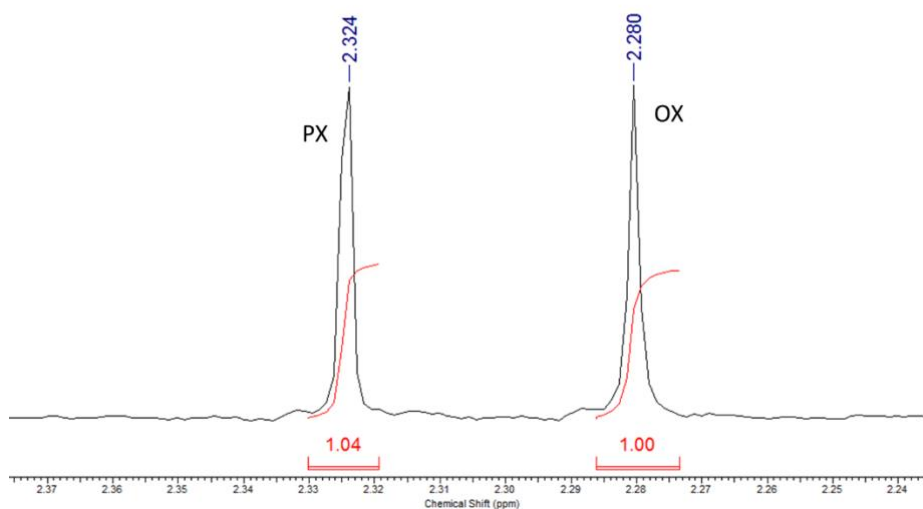


Figure S38. Magnified ¹H NMR spectrum recorded using the CDCl₃ extract of C₈ aromatics obtained from **sql-1,3-Co-NCS** that was prior subjected to the equimolar binary liquid of OX/PX until saturated.

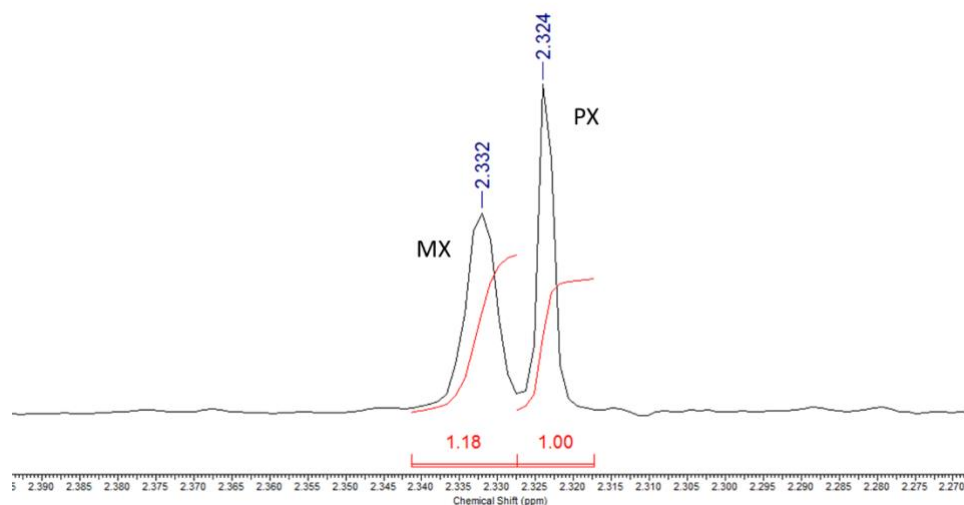


Figure S39. Magnified ¹H NMR spectrum recorded using the CDCl₃ extract of C₈ aromatics obtained from **sql-1,3-Co-NCS** that was prior subjected to the equimolar binary liquid of MX/PX until saturated.

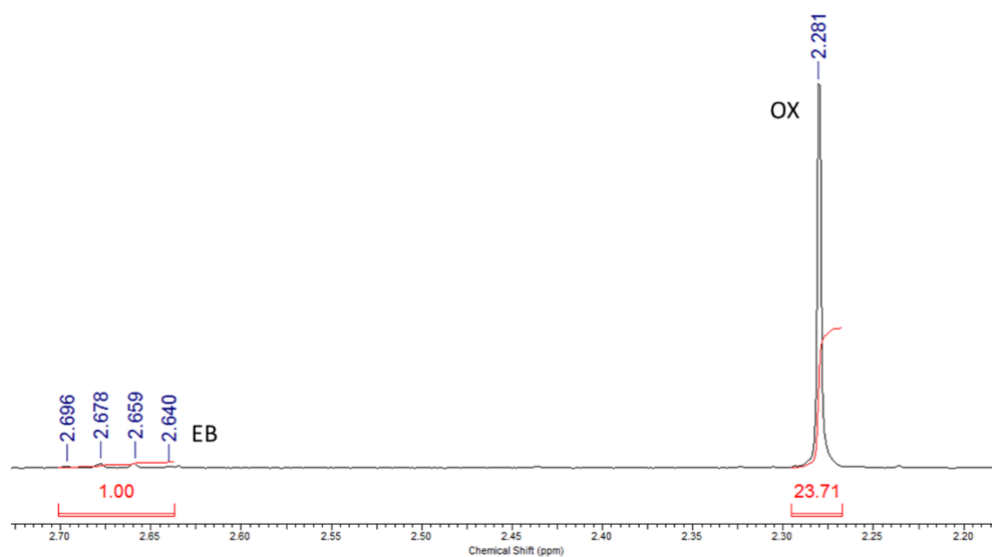


Figure S40. Magnified ¹H NMR spectrum recorded using the CDCl₃ extract C₈ aromatics from **sql-1,3-Co-NCS** that was prior subjected to the equimolar binary liquid of OX/EB until saturated.

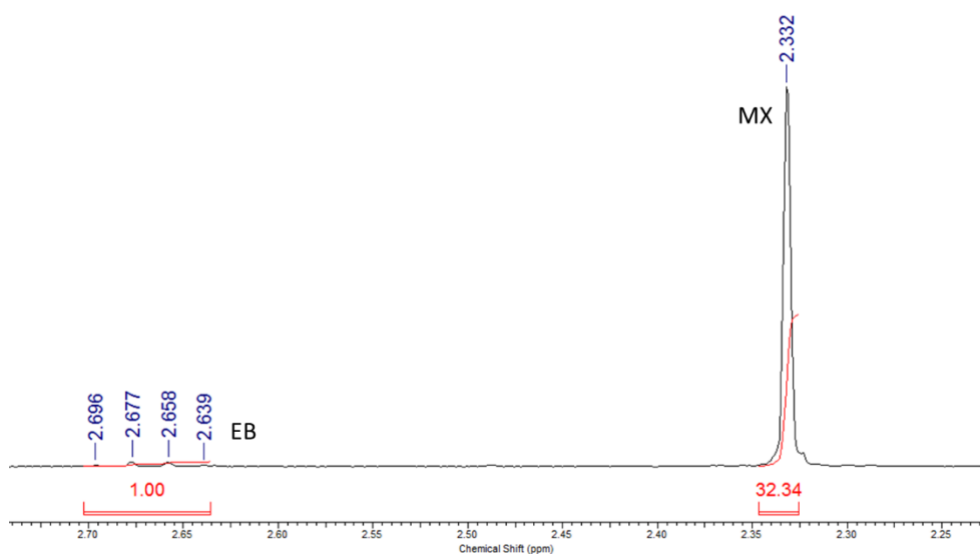


Figure S41. Magnified ¹H NMR spectrum recorded using the CDCl₃ extract of C₈ aromatics obtained from **sql-1,3-Co-NCS** that was prior subjected to the equimolar binary liquid of MX/EB until saturated.

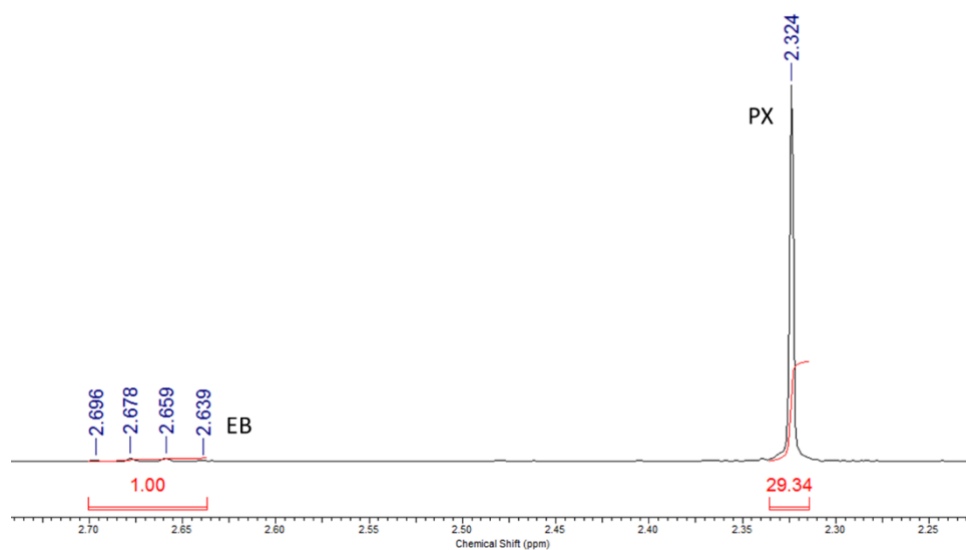


Figure S42. Magnified ¹H NMR spectrum recorded using the CDCl₃ extract of C₈ aromatics obtained from **sql-1,3-Co-NCS** that was prior subjected to the equimolar binary liquid of PX/EB until saturated.

Table S9. The uptake capacity and PX/EB, MX/EB and OX/EB selectivity for various adsorbents.⁴

Adsorbents	Uptake (wt%)					Selectivity		Ref./Note
	OX	MX	PX	EB	PX/EB	MX/EB	OX/EB	
sql-1,3-Co-NCS	37	37	37	18.7	9.8	10.8	7.9	Current work
sql-1-Co-NCS	87	87	87	43.5	7.3	3.8	60.1	4
BaX nanosize	4.9	2.02	10.34	3.15	3.745	NG.	NG.	15
KaX nanosize	4.2	1.8	10.1	3.2	3.22	NG.	NG.	16
[Ni(NCS) ₂ (ppp) ₄]	29	27	38	NG.	NG.	NG.	NG.	17
[Ce(HTCPB)]	NG.	12.7	11.7	NG.	2.4	NG.	NG.	18
JUC-77	0.9	2.3	33	NG.	NG.	NG.	NG.	19
MCF-50	NG.	NG.	NG.	NG.	NG.	NG.	NG.	20
Zn-MOF	0	0.11	0.42	NG.	NG.	NG.	NG.	21
ZIF-8	1.6	3.2	15.9	NG.	NG.	NG.	NG.	22
UiO-66	42.4	42.4	42.4	NG.	NG.	NG.	NG.	23
MIL-47 (V)	35	28	37	16	9.7	4.2	10.9	24
MIL-47 (V)	36	36	39	33	1.83	1.41	1.39	25
MIL-53(Al)	42	37.3	36.1	27.7	NG.	NG.	6.5	27
MIL-53(Al)	47.7	47.7	48.8	26.5	NG.	NG.	8.2	
MIL-53(Cr)	42.4	27.6	42.4	25.4	NG.	NG.	4.9	
MIL-53(Ga)	37.1	32.9	39.2	23.3	NG.	NG.	4.7	
MIL-53(Fe)	35	42.4	33.9	26.5	NG.	NG.	NG.	
MIL-53(Al)	46	26	43	17	3.1	3.8	10.9	28
MIL-53(Fe)	39	26	26	NG.	NG.	NG.	NG.	29
MIL-140B	12.7	12.7	12.7	12.7	2.1	NG.	NG.	30
MOF-48	27.6	27.6	27.6	27.6	1.5	NG.	NG.	
MOF-5	13	14.5	13	10	4.14	2.34	1.96	31
MOF-monoclinic	4.2	4.2	12.5	4.2	5.17	NG.	NG.	
Zn(BDC)(Dabco) _{0.5}	25	27	23	27	1/1.15	1.15	1.62	32
MIL-101 (Cr)	123	123	133	NG.	NG.	1/1.1	1.4	33, 34
CAU-13	17	15	14	NG.	NG.	NG.	NG.	35
MAF-X8	1.6	11.1	22.3	0	NG.	NG.	NG.	36
DynaMOF-100	0.53	2.12	31.8	3.82	NG.	NG.	NG.	37
MIL-125(Ti)-NH ₂	10	11	14.5	NG.	1.6	NG.	NG.	38
HKUST-1	29.7	25.4	29.7	NG.	NG.	NG.	NG.	39
CPO-27-Ni	20.1	22.3	21.2	NG.	NG.	NG.	NG.	
EtP5	0.2	1.1	8.9	NG.	NG.	NG.	NG.	40
EtP6	9.4	9.1	9.9	NG.	NG.	NG.	NG.	
H/ZSM-5	3.05	1.24	14.22	6.03	6.76	NG.	NG.	41
Li/ZSM-5	4.3	2.5	11	5.5	3.977	NG.	NG.	
Na/ZSM-5	3	2.5	9	5.5	2.008	NG.	NG.	
K/ZSM-5	2	1.2	8.3	7.5	1.101	NG.	NG.	
NaY microcrystalline	4	10	5	2	NG.	5.93	NG.	42
NaY nanocrystalline	4.2	11	4.5	1.1	NG.	6.88	NG.	
Co ₂ (dobdc)	38.2	36	35	35	1/3.21	1/2.05	1.21	43
Co ₂ (m-dobdc)	36	35.5	33.2	35.5	NG.	NG.	NG.	

Note: NG. means data not given; only the highest selectivity values were selected for the comparison.

Summary of structural parameters for sql nets

Table S10. Structural parameters for each sql net.

Compound	Square grid angles (°) ^a	∠Co-N-CS (°)	Torsion angle of bipy (°)	Interlayer separation (Å)
sql-1,3-Co-NCS·3EtOH (300 K)	90/ 90	168.8	36.7	4.700
sql-1,3-Co-NCS·2PX (301 K)	88.8/ 91.2	160.4	56.8	5.667
sql-1,3-Co-NCS·2MX (298 K)	90.6/ 89.4	157.1	54.8	5.707

^aThe square grid angles refer to adjacent ∠Co-Co-Co angles.

References

- V. A. Blatov, A. P. Shevchenko, D. M. Proserpio, *Crystal Growth & Design* 2014, **14**, 3576-3586.
- C. R. Groom, I. J. Bruno, M. P. Lightfoot, S. C. Ward, *Acta Cryst. B* 2016, **72**, 171-179.
- O. K. Farha, C. D. Malliakas, M. G. Kanatzidis, J. T. Hupp, *J. Am. Chem. Soc.* 2010, **132**, 3950-3952.
- S.-Q. Wang, S. Mukherjee, E. P.-Każmierczak, S. Darwish, A. Bajpai, Q.-Y. Yang, M. J. Zaworotko, *Angew. Chem., Int. Ed.* 2019, **58**, 6630-6634.
- APEX3. Ver. 2017.3-0. Bruker AXS Inc., Madison, Wisconsin, USA, 2017.
- L. Krause, R. Herbst-Irmer, G. M. Sheldrick and D. Stalke, *J. Appl. Cryst.* 2015, **48**, 3-10.
- XPREP Ver. 2014/2, Bruker AXS Inc., Madison, Wisconsin, USA, 2014.
- G. Sheldrick, *Acta Cryst. A* 2015, **71**, 3-8.
- G. Sheldrick, *Acta Cryst. C* 2015, **71**, 3-8.
- O. V. Dolomanov, L. J. Bourhis, R. J. Gildea, J. A. K. Howard, H. Puschmann, *J. Appl. Cryst.* 2009, **42**, 339.
- A. Boulouf and D. Lover, *J. Appl. Cryst.*, 1991, **24**, 987 – 993.
- W. I. F. David, K. Shankland, J. van de Streek, E. Pidcock, W. D. S. Motherwell, and J. C. Cole, *J. Appl. Cryst.*, 2006, **39**, 910 – 915.
- B.H.Toby, R.B.Von Dreele, *J. Appl. Cryst.*, 2013, **46**, 544-549.
- E. Jones, T. Oliphant, P. Peterson, *SciPy: Open source scientific tools for Python*, <http://www.scipy.org/> 2001.
- M. Rasouli, N. Yaghobi, F. Allahgholipour, H. Atashi, *Chem. Eng. Res. Des.* 2014, **92**, 1192-1199.
- M. Rasouli, N. Yaghobi, S. Z. Movassaghi Gilani, H. Atashi, M. Rasouli, *Chinese J. Chem. Eng.* 2015, **23**, 64-70.
- M. Lusi, L. J. Barbour, *Angew. Chem. Int. Ed.* 2012, **51**, 3928-3931.
- J. E. Warren, C. G. Perkins, K. E. Jelfs, P. Boldrin, P. A. Chater, G. J. Miller, T. D. Manning, M. E. Briggs, K. C. Stylianou, J. B. Claridge, M. J. Rosseinsky, *Angew. Chem. Int. Ed.* 2014, **53**, 4592-4596.
- Z. Jin, H.-Y. Zhao, X.-J. Zhao, Q.-R. Fang, J. R. Long, G.-S. Zhu, *Chem. Commun.* 2010, **46**, 8612-8614.
- J.-M. Lin, C.-T. He, P.-Q. Liao, R.-B. Lin, J.-P. Zhang, *Sci. Rep.* 2015, **5**, 11537.
- W. Huang, J. Jiang, D. Wu, J. Xu, B. Xue, A. M. Kirillov, *Inorg. Chem.* 2015, **54**, 10524-10526.
- M D. Peralta, G. Chaplais, J.-L. Paillaud, A. Simon-Masseron, K. Barthelet, G. D. Pirngruber, *Micropor. Mesopor. Mater.* 2013, **173**, 1-5.
- M. A. Moreira, J. C. Santos, A. F. P. Ferreira, J. M. Loureiro, F. Ragon, P. Horcajada, K.-E. Shim, Y.-K. Hwang, U. H. Lee, J.-S. Chang, C. Serre, A. E. Rodrigues, *Langmuir* 2012, **28**, 5715-5723
- L. Alaerts, C. E. A. Kirshhock, M. Maes, M. A. van der Veen, V. Finsy, A. Depla, J. A. Martens, G. V. Baron, P. Jacobs, J. F. M. Denayer, D. E. De Vos, *Angew. Chem., Int. Ed.* 2007, **46**, 4293-4297.
- V. Finsy, H. Verelst, L. Alaerts, D. De Vos, P. A. Jacobs, G. V. Baron, J. F. M. Denayer, *J. Am. Chem. Soc.* 2008, **130**, 7110-7118.
- V. Finsy, C. E. A. Kirschhock, G. Vedts, M. Maes, L. Alaerts, D. E. De Vos, G. V. Baron, J. F. M. Denayer, *Chem. – Eur. J.* 2009, **15**, 7724-7731.
- M. Agrawal, S. Bhattacharyya, Y. Huang, K. C. Jayachandrababu, C. R. Murdock, J. A. Bentley, A. Rivas-Cardona, M. M. Mertens, K. S. Walton, D. S. Sholl, S. Nair, *J. Phys. Chem. C*, 2017, **122**, 386-397.
- L. Alaerts, M. Maes, L. Giebeler, P. A. Jacobs, J. A. Martens, J. F. M. Denayer, C. E. A. Kirschhock, D. E. De Vos, *J. Am. Chem. Soc.* 2008, **130**, 14170-14178
- R. El Osta, A. Carlin-Sinclair, N. Guillou, R. I. Walton, F. Vermoortele, M. Maes, D. de Vos, F. Millange, *Chem. Mater.* 2012, **24**, 2781-2791.
- J. A. Gee, K. Zhang, S. Bhattacharyya, J. Bentley, M. Rungta, J. S. Abichandani, D. S. Sholl, S. Nair, *J. Phys. Chem. C* 2016, **120**, 12075-12082.
- Z.-Y. Gu, D.-Q. Jiang, H.-F. Wang, X.-Y. Cui, X.-P. Yan, *J. Phys. Chem. C* 2010, **114**, 311-316.
- M. P. M. Nicolau, P. S. Barcia, J. M. Gallegos, J. A. C. Silva, A. E. Rodrigues, B. Chen, *J. Phys. Chem. C* 2009,

- 113**, 13173-13179.
33. P. Trens, H. Belarbi, C. Shepherd, P. Gonzalez, N. A. Ramsahye, U. H. Lee, Y.-K. Seo, J.-S. Chang, *Micropor. Mesopor. Mater.* 2014, **183**, 17-22.
34. Z.-Y. Gu, X.-P. Yan, *Angew. Chem., Int. Ed.* 2010, **49**, 1477-1480.
35. F. Niekpiel, J. Lannoeye, H. Reinsch, A. S. Munn, A. Heerwig, I. Zizak, S. Kaskel, R. I. Walton, D. de Vos, P. Llewellyn, A. Lieb, G. Maurin, N. Stock, *Inorg. Chem.* 2014, **53**, 4610-4620.
36. A. Torres-Knoop, R. Krishna, D. Dubbeldam, *Angew. Chem. Int. Ed.* 2014, **53**, 7774-7778. 60.
37. S. Mukherjee, B. Joarder, B. Manna, A. V. Desai, A. K. Chaudhari, S. K. Ghosh, *Sci. Rep.* 2014, **4**, 5761.
38. F. Vermoortele, M. Maes, P. Z. Moghadam, M. J. Lennox, F. Ragon, M. Boulhout, S. Biswas, K. G. M. Laurier, Beurroies, R. Debovel, M. Roeffaers, N. Stock, T. Duren, C. Serre, D. E. De Vos, *J. Am. Chem. Soc.* 2011, **133**, 18526-18529.
39. D. Peralta, K. Barthelet, J. Pérez-Pellitero, C. Chizallet, G. Chaplais, A. Simon-Masseron, G. D. Pirngruber, *J. Phys. Chem. C* 2012, **116**, 21844-21855.
40. K. Jie, M. Liu, Y. Zhou, M. A. Little, A. Pulido, S. Y. Chong, A. Stephenson, A. R. Hughes, F. Sakakibara, T. Ogoshi, F. Blanc, G. M. Day, F. Huang, A. I. Cooper, *J. Am. Chem. Soc.* 2018, **140**, 6921-6930.
41. M. Rasouli, N. Yaghobi, S. Chitsazan, M. H. Sayyar, *Micropor. Mesopor. Mater.* 2012, **150**, 47-54.
42. M. Rasouli, N. Yaghobi, S. Chitsazan, M. H. Sayyar, *Micropor. Mesopor. Mater.* 2012, **152**, 141-147.
43. M. I. Gonzalez, M. T. Kapelewski, E. D. Bloch, P. J. Milner, D. A. Reed, M. R. Hudson, J. A. Mason, G. Barin, C. M. Brown, J. R. Long, *J. Am. Chem. Soc.* 2018, **140**, 3412-3422.